Contribution of the Lateral Collateral Ligament on Distribution of Forces in the Canine Elbow: An Ex Vivo Study

Candidate: Sorcha Rebecca Costello

A thesis submitted in fulfilment of the requirements for the degree of Masters of Veterinary Clinical Studies

For the Faculty Science, Sydney School of Veterinary Science

The University of Sydney 2026

Contents

Abstract

Title: Contribution of the lateral collateral ligament on Contact Mechanics in the Canine Elbow: An Ex Vivo Study

Objectives: Subchondral microfracture resulting from joint incongruency and overloading is hypothesised to be a contributing factor in the development of canine elbow dysplasia. While several osteotomy procedures aimed at modifying joint loading have been described, the influence of soft tissue stability warrants investigation. The objective of this study was to determine the effects of lateral collateral ligament (LCL) deficiency on load distribution within the joint, specifically contact force, pressure, and area between the medial and lateral compartments of canine cadaveric elbows under simulated axial loading during the stance phase. Additionally, this study aimed to evaluate whether prosthetic ligament reconstruction restores normal biomechanics within the joint.

Study Design: Ex-vivo cadaveric mechanical evaluation

Methods: Elbow joints (N=3) were subjected to four testing conditions using a non-constrained limb press model (condition A: intact LCL, condition B: cranial crus of the LCL transected, condition C: entire LCL transected, condition D: prosthetic LCL placed), with each condition tested in triplicate. Tactile array sensors placed in the medial and lateral compartment allowed continuous direct measurement of contact area, contact pressure and contact force. Limbs were loaded on a calibrated electromechanical testing system to 200 N under each testing condition at a 135-degree standing angle.

Results: Force and contact pressure within the medial compartment increased as a result of full transection of the LCL when compared as a proportion to the lateral compartment ($P = 0.023$ and $P = 0.045$ respectively). Placement of a prosthetic LCL did not restore normal intra-articular joint contact mechanics. No significant change in contact area was observed between testing conditions.

Conclusion: A LCL deficient elbow results in increased forces within the medial compartment, prosthetic ligament placement does not entirely restore normal elbow biomechanics. Prosthetic ligament placement may reduce loading of the medial compartment; however, the technique requires further development to reduce variability in loading effect.

Statement of Originality

This is to certify that to the best of my knowledge; the content of this thesis is my own work. This thesis has not been submitted for any other degree or other purposes.
I certify that the intellectual content of this thesis is the product of my own work and that all assistance received in preparing this thesis and sources have been acknowledged.

No generative artificial intelligence (AI) tools were used in the research, analysis, or preparation of this thesis.

This research was supported by an Australian Government Research Training Program (RTP) Scholarship.

Sorcha Rebecca Costello
Date: 23/12/2024

Chapter 1

1.1 Background

Elbow dysplasia is an umbrella term encompassing multiple diseases of the canine elbow joint. The term first appeared in the veterinary literature in 1961, and was later formalised by the International Elbow Working Group (IEWG) in 1993 (1,2). Elbow dysplasia manifests in one or more of the following: ununited anconeal process, elbow incongruity, fragmented medial coronoid disease, and osteochondrosis (osteochondritis dissecans) of the medial humeral condyle (3). The pathophysiology of elbow dysplasia is not fully understood, but both genetic and environmental factors play significant roles in the incidence and severity with joint incongruency and regional overloading suggested as the cause in most cases (3). Lameness and pain develop in most dogs before one year of age resulting in degenerative joint disease primarily affecting the medial compartment as the disease progresses (4).

1.1.1 Aetiology and Epidemiology of Canine Elbow Dysplasia

The aetiology of canine elbow dysplasia is multifactorial, with varying degrees of severity, determining the development of the disease in each individual. Elbow dysplasia is the most common condition found in dogs presenting with thoracic limb lameness. It affects mostly large and giant breeds such as Labradors, German shepherd dogs, Staffordshire bull terriers, and rottweilers but also chondrodysplastic breeds such as dachshunds and French bulldogs (5,6). Lameness identification can be challenging with 35-88.4% of dogs being bilaterally affected (5–7). Clinical signs may be seen in immature dogs or in some cases, not until maturity when secondary degenerative disease has advanced (6,8–10).

Elbow dysplasia in dogs is considered a hereditary condition with a polygenic mode of inheritance. More male dogs are affected than females, it is suspected sex distribution is associated with dominant inheritance in the male lineage (3,4). The incidence of the disease is high in some breeds such as the Bernese mountain dog, Labrador, and Newfoundland with 70, 17-29, and 26% of the respective populations affected (5). Several epidemiological studies investigating the genetic contribution to the development of elbow dysplasia show breed difference inheritance pattens. Additionally, each component of the disease can be inherited independently making genetic testing for the condition especially challenging (11,12). Screening schemes have been adopted to reduce the incidence of disease. When one parent has elbow dysplasia, the risk of developing disease doubles from 10-23% with this risk shown to increase with severity of disease of the parents (13). The Australian veterinary association (AVA) and the Australian national kennel club (ANKC) developed the canine hip and elbow dysplasia scheme (CHEDS) in January 2000. This is similar to schemes used worldwide and generates a quantitative score for dogs over 12 months of age heavily weighted towards secondary degenerative changes. The PennHIP scheme, for hip dysplasia, is now more widely accepted than its elbow counterpart due to its use in dogs as young as four months to predict the development of secondary changes. Similar schemes for elbow evaluation are yet to be developed (14). Environmental factors impact both genetic expression and phenotype development. Diet, body weight, housing and activity levels are thought to contribute to the degree of trauma to the elbow joint influencing progression of secondary degenerative changes but do not impact the prevalence of elbow dysplasia (15,16).

1.1.2 Anatomy of the Canine Elbow

The canine elbow joint is a complex synovial trochleoginglymoid joint comprised of the humerus, radius, ulna, and soft tissue structures (17). The medial and lateral distal humeral condyles are referred to as the trochlea and the capitulum. They articulate with the ulna and radial head respectively (18). From these bony structures, three articulations are formed: the humeroradial joint, the humeroulnar joint, and the radioulnar joint. Supporting these bony articulations are soft tissue structures that provide passive support – joint capsule, ligaments, and tendons as well as muscles providing active support (19–22).

Three main ligamentous structures comprise the canine elbow joint. They are comprised primarily of type I collagen (90%) but also type III collagen, water, proteoglycans, elastin, and several other biomechanical substances (23). The collagen fascicles are densely packed in a parallel arrangement with a slight crimp pattern which allows for only slight elongation without damage (23).

The annular ligament connects the radius and the ulna. It is a broad, fibrous band that originates from the ulna on the lateral aspect of the joint, cranial to the lateral coronoid process where it blends with fibres of the lateral collateral ligament (LCL). It then courses over the radial head where the inner surface cartilaginous lining contacts the radial head to then attach at the craniodistal border of the medial collateral ligament (MCL) (10).

There are two collateral ligaments, medial and lateral (MCL and LCL). These originate proximally on the medial and lateral humeral epicondyles respectively and go to divide into two crura distally. For both ligaments, the cranial crura attach to the radius and the caudal crura attach to the ulna. Because there is only a fibrous joint capsule on the cranial aspect of the elbow joint, these caudal crura are considered thickenings of the joint capsule. Additionally, the lateral collateral crura blend with the annular ligament and in some dogs can contain a sesamoid bone which can be seen radiographically (18–20,23,24). The caudal crura of the MCL traverses to penetrate the interosseus space attaching to the proximal caudolateral surface of the radius caudally to the insertion of the cranial portion of the LCL (23). Experimentally, the LCL has shown to be significantly stronger and stiffer than the MCL despite similar mechanical properties (24).

These structures interact together to allow the joint to function as a hinge joint with some pivot articulation seen as pronation and supination of the antebrachium (21,22). The normal range of motion of the canine elbow joint is 30-60 degrees (18).

- The humeroulnar joint is responsible for restricting movement to the sagittal plane and allows flexion and extension (25).
- The humeroradial joint is responsible for 52% of weight-bearing (25,26).
- The proximal radioulnar joint is where the radius articulates with the medial coronoid process at the radial incisure. This is where the radius can supinate and pronate and is responsible for 48% of weight-bearing (25,26).

1.1.3 Stabilisers of the Canine Elbow

The stability of the joint is provided by both intrinsic and extrinsic components. The complex shapes of the articular surfaces' provides intrinsic support, whilst the periarticular soft tissues give extrinsic support. Stabilisers have been described as primary, secondary, or tertiary depending on the level of restraint they provide to any given displacement. Primary stabilisers being 33%, secondary 10-33%, and tertiary less than 10% (27). Defining stabilisers of the joint

allows understanding of the function of these elements in relation to how a deficiency in any of these can contribute to clinical disease. The anconeal process is a primary stabiliser and provides the greatest resistance to pronation. The LCL is also a primary stabiliser providing the greatest resistance to supination but also acts as a secondary stabiliser to provide rotational stability. The MCL is a secondary stabiliser to pronation (27). This can be assessed clinically with the Campbell test where the shoulder and elbow are flexed at 90 degrees and rotational forces are placed to supinate or pronate the elbow joint. The normal range of pronation in cadavers is 40-50 degrees and supination is 60-70 degrees (28). A MCL deficient elbow will pronate to 100 degrees and a LCL deficient elbow will supinate to 120-140 degrees (28) although Farrell et al. (2007) later concluded that these values are not absolute and can vary with the weight of the dog and recommends to compare angles with the contralateral limb (29). These changes in stability result in displacing loads within the joint such that a lateral collateral deficient elbow is likely to displace load to the medial compartment (27).

1.1.4 Pathophysiology of Elbow Dysplasia in Dogs

Elbow dysplasia was first described as a triad of lesions that can be solitary or in combination. Medial coronoid process disease (MCPD), osteochondrosis +/- osteochondrosis dissecans and ununited anconeal process (5,30,31). Medial coronoid disease is by far the most common of these lesions (8,10,32). Medial coronoid disease describes the erosion of the articular cartilage and subchondral bone pathology of the medial coronoid process which can progress to fracture, i.e. fractured medial coronoid process (FMCP) (9,25). This occurs secondary to increased mechanical loading of the medial compartment of the joint. It is therefore now accepted that MCPD is a specific lesion within a wider area of pathology affecting the whole medial compartment – this is termed medial compartment disease (9,25).

The exact pathophysiology is still under investigation and several theories exist as to what causes overloading of the medial compartment. Three suggested mechanisms include biomechanical force mismatch, incongruency of all three joint components and disorders of endochondral ossification (3).

Radioulnar incongruency – associated with asynchronous growth of the radius and ulna resulting in a step radioulnar joint (positive radioulnar incongruence). This malalignment of articular surfaces alters contact areas of the joint altering compression, shear, and rotational forces shifting mechanical load to the medial compartment (9,25,31,33,34). This incongruency has been observed in 14-100% of elbows with FMCD (35–39). The wide range of reported incidence of incongruency in dogs with FMCD may be due to lack of diagnostic sensitivity and contributions of other mechanisms explained by the concept of dynamic radioulnar longitudinal incongruency. This theory hypothesises that under normal loading, there is a dynamic step formation within the radioulnar joint which is not detectable with conventional imaging while the joint is not loaded (7,40,41). Rohwedder et al. showed that the radioulnar joint conformation changes significantly in sound elbows during locomotion and static radioulnar incongruence persists in dogs with MCD at a walk. The group also showed that in orthopedically healthy animals a negative radioulnar incongruency appears whilst at a walk – this is where the radius is long placing more pressure on the anconaeus (7,25). This supports the theory of dynamic radioulnar incongruency causing medial compartment disease.

Humeroulnar incongruency is associated with the shape of the ulnar trochlear notch i.e. a mismatch between the trochlear notch and the humeral condyles or a long radius which displaces the humerus from the ulnar notch (25,33,40). Forty percent of dogs seen to have humeroulnar incongruency have MCPD (5).

Musculotendinous mismatch is also hypothesised to play a role contributing to instability of the joint. Alterations in these surrounding supporting structures can lead to altered intraarticular loading. Primary rotational instability of the radius and ulna relative to the distal aspect of the humerus can result in instability and incongruence through all or part of the range of motion (33). Elbow luxation has been shown to be caused by forces produced from the supinator muscle in conjunction with under development/laxity of the LCL or annular ligament (42). In this case, joint instability and altered loading surfaces are thought to have progressed to the extreme of elbow luxation (42).

The biceps brachii muscle originates from the supraglenoid tuberosity to insert in two parts at the elbow joint, the larger part on the ulnar tuberosity and the smaller on the radial tuberosity. The moment produced by contraction of the muscle rotates the craniolateral segment of the medial coronoid process against the radial head to compress the medial coronoid process against the radial head. This generates shear stress and repeated loading to the medial coronoid (31,40).

Although it cannot be agreed on the exact mechanism to medial compartment disease it is likely to be a multifactorial disease, advances in research have helped deduce what is happening within the joint as a result of abnormal loading to cause MCD progress to FMCP. Excessive pressure on the medial coronoid leads to fatigue by way of microcracks in the subchondral bone compromising the mechanical properties and leading to microfractures (6,34) Histologically, the subchondral bone of the medial compartment shows diffuse damage with osteocyte loss and increased porosity. Danielson and colleagues hypothesise that mechanical overload damages the bone injuring osteocytes and disrupting the canalicular network which in turn interferes with lacunocanalicular fluid flow and subsequent osteocyte nutrition. This leads to acute necrosis and apoptosis which is seen to a greater degree at the craniolateral edge (radial incisure) of the coronoid process where we see fragmentation (6,10). This process implies that FMCP disease is a primary lesion of the subchondral bone, and cartilage changes often seen on arthroscopy, are secondary (6). Bone mineral density of the axial portion of the medial coronoid process to be reduced by 50% compared to the abaxial region. As compressive strength of bone is proportional to the square of its density, this would equate to a 4 fold decrease in compressive strength which leads to fragmentation and eventually fractures seen in these diseased dogs (8). Subchondral pathology will therefore precede changes to articular cartilage and subsequent secondary changes including osteoarthritis which cannot be reversed (40).

1.1.5 Diagnosis of Medial Coronoid Disease

Suspicion of MCPD with signalment, history, and a physical examination. These dogs often present with a reduced range of motion of the elbow, discomfort on hyperextension of the elbow and pain on external rotation of the carpus. Joint effusion is proportional to the severity of synovitis due to exposed subchondral bone and can be palpated under the anconaeus muscle (25,43). In severe cases when secondary degenerative changes occur, periarticular swelling and crepitus in extension can be observed (43). When standing patients will display a bow-legged stance with external rotation of the limb which is adopted as the dog attempts to offload the medial compartment and direct forces laterally. In particularly stoic dogs, pain can usually be elicited by palpating the medial coronoid process when applying pressure approximately 1cm distal to the medial humeral epicondyle (25).

Due to the pathological process described above, no imaging modality is 100% sensitive for the diagnosis of medial compartment disease. Radiography, CT, and MRI cannot identify dynamic incongruity whereas arthroscopy can detect damage to articular cartilage, but not the pathology to the underlying subchondral bone which precedes this (25).

Radiography

Radiography is widely available in most veterinary practices and will generally be the first diagnostic step in investigations for suspected elbow dysplasia. Radiography can be challenging as it is a 2D image and thus limited due to the superimposition of the medial epicondyle and muscle tissues (5). Due to the complexity of the joint, maximising radiographic data requires evaluation of four projections of both elbows:

- Mediolateral neutral view with the elbow at 120 degrees.
- Mediolateral flexed view with the elbow at 45 degrees.
- Craniocaudal view.
- Craniocaudal oblique view with the antebrachium at 15 degrees of pronation (43,44).

Radiographically, evidence of MCPD is seen with features such as an indistinct or deformed contour of the medial coronoid process, sclerosis of the distal section of the semilunar notch, and loss of trabecular pattern and/or reduced opacity of the medial coronoid process (32). Radioulnar incongruity is observed as radioulnar length disparity and an uneven joint rim between the humeral condyle and radial head as well as a step between the articular surfaces (43). Diagnosis of incongruency by radiography was shown in one cadaveric study to be imprecise requiring a 1.5-4mm step to achieve 86% specificity and 90% sensitivity for diagnosis (38). As the disease progresses into elbow osteoarthritis, osteoarthritic changes such as osteophytes can be scored based on size as mild, moderate, or severe (32). At the time of diagnosis up to 57% of dogs already have concurrent osteoarthritis which can be seen radiographically (5). The long pathogenesis of the disease likely accounts for the range in sensitivity reported for radiographic diagnosis of 10-62% (32).

CT

CT provides cross-sectional images which allow differentiation between superimposing structures and distinguishes tissues of various densities to obtain volumetric data. CT can detect changes in shape, attenuation, fragmentation, or fissures of the coronoid process as well as trochlear notch sclerosis and irregularities of the joint space (32).

CT provides evaluation of subchondral bone changes associated with early disease however does not allow imaging of the articular cartilage (44). Though more sensitive than radiography, the most accurate assessment of pathology in the elbow has been shown with a combination of CT and arthroscopy. When combined, CT and arthroscopy provide a sensitivity of 100% and specificity of 93% (8,32).

Arthroscopy

Arthroscopy allows direct visualization of the articular cartilage and is the gold standard in human and veterinary medicine for elbow joint evaluation. It allows for the evaluation of fissures, fragmentation, and chondromalacia. (32). The Outerbridge classification system is used to score the condition of the articular cartilage and can assist with treatment decisions and predict disease progression. The modified Outerbridge classification system is based on the degree of cartilage loss within the joint and is scored from 0-4.

- 0 – normal cartilage

- I – chondromalacia
- II – fibrillation and damage to the superficial matrix only
- III – full-thickness fissure and loss of cellular components
- IV – full thickness erosion of cartilage to the level of the subchondral bone.

These scores will guide treatment as scores I and II are reversible and with appropriate interventions, fibrocartilage replaces the defects seen in arthroscopy. Scores III and IV, however, are progressive due to the underlying subchondral bone damage, and even with debridement or load shifting treatments disease will progress therefore load modifying techniques alone will not stop the progression of osteoarthritis (4,40).

Arthroscopy can only evaluate the articular cartilage and has been shown to miss fissures or fractures which are still covered with articular cartilage. This is why arthroscopy should be used in conjunction with CT (45).

1.1.6 Treatment of Medial Compartment Disease

It is well recognised that early treatment will result in better outcomes and long-term prognosis for limb function however this relies on diagnosis before the development of progressive pathology in the subchondral bone which regardless of treatment will extend to osteoarthritis. Outcomes have shown in these cases to be similar, regardless of treatment, with an initial improvement of lameness and pain scores however follow-up radiographs and clinical outcomes show the progression of osteoarthritis and decreased range of motion of the affected joints. This is because, as described above, the pathology extends to a greater extent and the disease is diffuse affecting much of the medial compartment (6).

This leads to point the failures in diagnosis and treatment of this condition and highlights areas that need development. That is, diagnostics to detect pathology before subchondral bone damage and less technical treatments that can subsequently off-load the medial compartment to stop the progression of the disease and allow for healing. These treatments must be performed within the window of reversible damage.

Conservative management is not often opted for as a sole treatment except for old dogs or those with comorbidities increasing surgical risk. Conservative management should be used in conjunction with surgery and includes weight control, activity restriction (with low impact activity encourage and high impact activities avoided), omega 3 essential fatty acids (EFAs), NSAIDs, non-opioid analgesics (gabapentin, amantadine), joint supplements (glucosamine and chondroitin) and injectable medications (polysulfated glycosaminoglycans), intraarticular injections (hyaluronate and corticosteroids), regenerative medicine (stem cells, PRP), laser therapy and external beam radiation or radiation delivered through intra-articular injection such as Synovetin OA (available in the USA) (4).

Surgical treatment can be grouped by the surgical aim:

- Removal of fracture fragments of the medial coronoid process or ostectomies at fissure lines
    - Arthrotomy/arthroscopy +/- subchondroid ostectomy or fragment removal (4)
- Correct elbow incongruency
    - Distal ulnar ostectomy
    - Proximal ulnar ostectomy
    - Bi-oblique ulnar osteotomy
- Offloading the medial compartment with soft tissue techniques

- Offloading the medial compartment with shifting osteotomies
    - Sliding humeral ostectomy (SHO)
    - Proximal abducting ulnar ostectomy (PAUL)
- Resurfacing
    - Canine unicompartmental elbow arthroplasty (CUE)
- Replacement
    - BANC PER – biomechanically non-constrained compartment partial elbow replacement (Kyon)
    - Total elbow replacement

Fragment Removal

Several studies have compared outcomes between arthrotomy, arthroscopy, fragment removal and subchondroid ostectomy. One prospective study with low case numbers did not show a difference in outcomes with dogs treated conservatively and arthroscopically (46). Subchondral ostectomy is thought to address disease of the subchondral bone associated with continuing joint pain which is not addressed with fragment removal alone however in one study, it was reported to accelerate cartilage loss (47).

Ulnar Ostectomies and Osteotomies

Distal ulnar ostectomies can be performed in skeletally immature dogs with premature physeal closure at the distal ulnar growth plate. The purpose is to allow the radius to grow unconstrained by the ulna. At skeletal maturity, a proximal ulnar osteotomy or bioblique dynamic proximal ulnar osteotomy can be performed. Incongruity is addressed spontaneously during weight bearing with axial migration and three-dimensional rotation of the proximal ulnar segment (48). Long term outcomes suggest both distal and proximal ostectomies and osteotomies improve load distribution within the joint but result in reduced range of motion and progression of osteoarthritis (49).

Biceps Ulnar Releasing Procedure (BURP)

This technique involves a partial release of the biceps tendon at the level of the ulna to neutralise the compressive forces on the medial coronoid. Although described, there are currently no controlled studies to evaluate the procedure, complications and outcomes (3).

Sliding Humeral Osteotomy

The purpose of this procedure is to shift the weight bearing axis of the thoracic limb laterally to offload the medial compartment. The literature assessing medium and long-term outcomes is limited with major complication rates ranging from 4.17-18.75% with good to excellent outcomes in regards to lameness at 12 weeks owner assessment (50,51).

Proximal Abducting Ulnar Osteotomy

This technique is aimed at addressing medial collapse of the joint in patients with medial coronoid disease. Abducting the ulna by 4-6 degrees, unloads the medial compartment, reduces pain and slow disease progression. After an osteotomy is performed in the proximal ulna, a PAUL plate with a 2-3mm step is applied to the lateral surface which lengthens the ulna resulting in a load shift to the lateral compartment during weight bearing. This procedure is palliative and not appropriate for patients with degenerative changes to the lateral compartment (4). Outcomes are patient dependent, related to the severity of disease at the time of surgery with long term data suggesting 89% of patients have full return to weight bearing or only

occasionally lame. Second look arthroscopy in two dogs showed growth of articular fibrocartilage where previously full thickness erosion was noted pre-operatively (4,52).

Canine Unicompartmental Elbow Arthroplasty

The rationale of this procedure is to preserve stabilisers of the elbow and maintain load transmission in a complex joint. Unilateral resurfacing prevents stimulation of nociceptors within subchondral bone during bone to bone loading in cases of advanced disease. Outcomes at 4-6 months suggest acceptable comes with major/catastrophic complication rates of 11.7% (53).

Elbow Replacement

Prosthetic arthroplasty requires range of motion in the sagittal plane as a hinge joint whilst allowing for pronation and supination during locomotion. Constraint is the mechanical linking of the articulations within the joint, the elbow has three separate articulation compartments. Prosthetic arthroplasties are classified as constrained, semi constrained or non-constrained (4).

Biomechanically non-constrained compartment partial elbow replacement systems allow replacement of only the affected compartment or conversion to the total elbow replacement system if both compartments are affected.

Total elbow replacement in dogs was first described in 1989 and since this time systems have evolved to address unacceptable outcomes associated with implant design. The ideal prosthetic design has not yet been achieved and research is still on-going. Complication rates are still suboptimal and revision options are limited however replacement may be an option for cases with severe or end-stage disease (4).

1.2 Introduction to the Current Study

Treatment aimed at correcting the underlying pathophysiology prior to the onset of progressive disease remains a challenge. The basis of early surgical interventional techniques, i.e. ulnar ostectomies/osteotomies and offloading techniques, rely on altering the elbow biomechanics and forces acting within the joint. Intra-articular forces have been previously investigated by several methods.

Joint casting is where polymethyl methacrylate is injected into the joint space and the joint is compressed as axial force is applied to the limb. This method can identify contact areas within the joint but cannot detect the degree of forces or their distribution (22,34). With this method, three continuous contact areas were identified within the joint – the radial head, the craniolateral aspect of the anconaeus, and the medial coronoid process (34). The key limitation of this technique is the lack of data on the distribution and quantitative force experienced within the joint. This is overcome by the use of digital pressure sensors placed within the joint. Mason and colleagues used pressure sensors, placed with cadaver elbows to investigate the quantitative distribution of force between the articular surfaces of the humerus and radius and humerus and ulna in normal canine elbows. Limbs were loaded with axial force applied at various strengths (5 N, 100 N, 150 N, and 200 N) in a custom rig mechanism. They showed an even distribution of pressures within the medial and lateral compartments of the normal elbow with the ulna contributing substantially to load transfer (26).

Preston and colleagues went on to see the effects of incremental radial shortening (i.e. introducing an incongruency) and ulnar osteotomies (i.e. a common surgical treatment to

restore congruity). They confirmed that as incongruency was introduced by radial shortening, the radial contact area became smaller, the anconeal contact area disappeared entirely and the medial coronoid contact area remained but migrated craniolaterally toward the radial incisure. This was then dynamically stabilised with an ulnar ostectomy proximal to the interosseus ligament (54)

Krotscheck and colleagues aimed to determine the effect of elbow congruity on contact mechanism and the effect of subsequent treatment of the incongruity with one or two ulnar ostectomies – PUO or DUO. In agreement with Preston et al., they showed that radial shortening shifts both the mean contact pressure and the peak contact pressure from the lateral to medial compartments (9). In a normal elbow, there is an even distribution of pressures between the medial and lateral compartments (22,26). After PUO the mean contact pressure within the medial compartment was normalised and the peak contact pressure was decreased which may be of further benefit to these patients. DUO will also have contact pressures return to baseline if concurrently the interosseous ligament is transected and the ulnar attachment of the abductor pollicus muscle is released (9).

As we know from the evolving field of total elbow replacements, the elbow is complex and cannot be thought of as just a hinge joint. The articulations and supporting structures allow some degree of pronation and supination in addition to sagittal motion. For this reason, Cuddy et al. evaluated how antebrachial rotation at different flexion angles affects the contact mechanisms within a normal elbow. This was to better emulate the forces that would act within the joint during the gait cycle. As with Mason's study above, pressure sensors were placed in the medial and lateral compartments and the limb was loaded with 200N in a custom jig. The limb was manipulated in different positions of flexion (115, 135, and 155 degrees, as well as different degrees of pronation and supination. Cuddy et al. showed that both pronation and supination increase peak contact pressure and decrease contact area in both the medial and lateral compartments. It is hypothesised that peak contact area increases due to the relative tightening of the joint when the medial and LCLs become more taught during these maneuverers. Pressure mapping showed that the area of peak contact shifted further from the apex of the medial coronoid in supination and closer in pronation. As the limb is in supination, there is a significant translation of the apex of the medial coronoid caudally and external rotation relative to the radial head (22). This fits with the theory that the medial coronoid experiences repeated microtrauma caudally and abaxially leading to radial incisure location fissures (22). This location agrees with previously discussed histomorphology studies showing this region to be the most significantly affected (6).

Evidence that it is not just axial force, but compressive, shear, and rotational forces that are a result of myotendinous stabilisers which determine the contact area across the cartilage interface. Hulse et al. previously investigated the role of the biceps muscle on articular structures concluding that the biceps acts to stabilise the joint concurrently compressing the medial compartment (31). This suggests joint stabilisers can be utilised to manipulate load pressures away from the medial compartment. By addressing abnormal load early it is possible to decrease or reverse arthroscopic evidence of cartilage loss – as has been shown for offloading techniques (4). The lateral collateral is a primary stabilizer of the elbow providing resistance to abduction and internal rotation (55). There are no current publications on the contribution of the LCL to joint surface contact area or pressures. Further research in this area may lead to a new way in which we treat elbow dysplasia early in the course of the disease as well as aiding in the development of superior total elbow joint arthroplasty systems.

This study introduces the concept that the LCL, as a primary stabiliser of the elbow, influences elbow biomechanics and may also contribute to rotational instability of the humerus in the dog. Laxity of the LCL may be a contributor to the musculotendinous mismatch theory of medial compartment disease in dogs with elbow dysplasia. The aim of the present study was to evaluate the contribution of the LCL on the biomechanics of the canine elbow joint. The hypothesis is instability related to the LCL results in the joint force reduction in the lateral compartment and subsequent redistribution of force into the medial compartment. Ligament laxity may contribute to altered loading within the joint of dogs resulting in stress microfractures in the medial coronoid subchondral bone and subsequent pathology observed in dogs with medial compartment disease.

Chapter 2

Selecting and Obtaining Cadaveric Specimens and Cadaveric Processing Technique

2.1 Specimen Selection

Cadavers were obtained through The University of Sydney Animal Donation Program. Dogs were euthanized for reasons unrelated to the study and used in accordance with guideline GL001 from the institution's animal ethics committee.

Skeletally mature non-chondrodystrophic cadavers in apparent good health prior to euthanasia were selected based on availability with the Animal Donation Program. Preference was given to younger animals at the time of euthanasia to reduce exclusion due to elbow pathology during the screening process. At the time of selection, whole cadavers were frozen at -20°C at The University of Sydney and defrosted for the study based on records stored within the Animal Donation Program. Records available for cadaver selection prior to defrosting were most often limited to the size, species and suspected breed.

Figure 2.1.1: Cadavers extracted from The University of Sydney Animal Donation Program showing the identification tag used to obtain the limited data available regarding the animal prior to euthanasia.

Data were recorded on an Excel spreadsheet with each dog having an identification number and left and right legs recorded as A or B respectively. The breed of dog and weight was recorded as well as evidence of pathology radiographically or on visual inspection of the joint (Table 2.1).

2.2 Specimen Collection

Cadavers were thawed over a period of five days at a temperature of 5°C to minimise the impact of autolysis on the integrity of the soft tissues. Once thawed, the thoracic limbs were clipped of fur with a size 40 blade and amputated with a standard forequarter amputation described below:

1. A skin incision was made with a size 10 scalpel blade circumferentially around the periphery of the scapular to join medially at the axilla at the level of the shoulder joint.
2. The subcutaneous tissues were bluntly dissected with Mayo scissors on the lateral aspect to the muscular insertions on the scapular.
3. The ventral margin of the omotransversarius muscle cranial to the acromion process was undermined with Mayo scissors extended cranially to the level of the trapezius muscle dorsal to the scapular spine. The muscle attachments to the scapular spine were transected with a size 10 scalpel blade.
4. The scapula was grasped with a towel clamp and elevated to facilitate transection of the attachments of the rhomboideus and serratus ventralis muscles.
5. The brachial plexus and axillary vessels were transacted with Mayo scissors and ligated if required to reduce contamination of blood.
6. The remaining subcutaneous tissue attachments were dissected with sharp dissection with Mayo scissors on the caudal aspect and upper thoracic limb.
7. The limb was internally rotated to isolate the latissimus dorsi which was transected with Mayo scissors at its attachment to the medial brachial fascia.
8. The limb was externally rotated to transect the cleidobrachalis muscle near the greater tubercle of the humerus.
9. The medial aspect of the limb was then exposed to facilitate transection of the tensor fascia antebrachia muscle, superficial and deep pectoral muscles.

2.3 Specimen Screening

Thoracic limbs then were wrapped in 0.9% NaCl solution soaked laparotomy sponges and sealed in double plastic bags for transport to an imaging facility. A minimum of three view radiographic projections were obtained of each thoracic limb to screen for evidence of joint disease. Limbs with evidence of elbow disease were excluded from the study.

Radiographic views obtained included:

- Mediolateral neutral projection.
- Mediolateral flexed projection.
- Craniocaudal projection.

Radiographs were assessed initially by the primary investigator and limbs were excluded if there was any overt evidence of pathology at the level of the elbow joint. Final radiographic assessment was performed by an ACVS and ECVS surgical specialist with extensive orthopaedic experience prior to inclusion in the study.

Limbs were excluded if any of the following was identified on the radiographic projections:

- Osteolytic or osteoproliferative lesions of the bone.
- Changes to soft tissue architecture including but not limited to masses or calcification.
- Subchondral sclerosis of the subtrochlear notch with loss of a trabecular pattern and a less defined increase in density.

- Ostophytosis of any aspect of the joint – most commonly the anconeal process, the lateral humeral condyle and the cranial aspect of the radial head.
- Incongruity between the ulna, radius and humeral condyles showing as an uneven joint rim or a step.

A selection of examples of radiographic projections of specimens included in the study are shown in Figure 2.3.1 below. Annotated radiographic examples of specimens excluded in the study are shown in Figure 2.3.2 and 2.3.3 below.

ID	Breed	Weight (kg)	Leg	Radiographic Evidence of Elbow Pathology	Excluded
1	Maltese cross breed	5.7	A	Palpable disease prior to radiography	Yes
			B	Palpable disease prior to radiography	Yes
2	Chihuahua	7.4	A	Palpable disease prior to radiography	Yes
			B	Palpable disease prior to radiography	Yes
3	Jack Russel Terrier	7.2	A	Palpable disease prior to radiography	Yes
			B	Palpable disease prior to radiography	Yes
4	Staffordshire Bull Terrier	12.7	A	Palpable disease prior to radiography	Yes
			B	Palpable disease prior to radiography	Yes
5	Staffordshire Bull Terrier	26.9	A	Palpable disease prior to radiography	Yes
			B	Palpable disease prior to radiography	Yes
6	Staffordshire Bull Terrier	29.1	A	No	No
			B	No	No
7	Chihuahua	11.9	A	Palpable disease prior to radiography	Yes
			B	Palpable disease prior to radiography	Yes
8	Terrier cross breed	16.4	A	Palpable disease prior to radiography	Yes
			B	Palpable disease prior to radiography	Yes
9	German Shepherd Dog	13.9	A	Palpable disease prior to radiography	Yes
			B	Palpable disease prior to radiography	Yes
10	Staffordshire Bull Terrier	35	A	No	No
			B	No	No
11	Great Dane	50.4	A	No	Yes
			B	No	Yes
12	Siberian Husky	24.3	A	Amputee	N/A
			B	No	No
13	Greyhound	28.4	A	No	No
			B	No	No

14	Chihuahua	11.9	A	No	No
			B	No	No
15	Siberian Husky	22.2	A	No	No
			B	No	No
16	Staffordshire Bull Terrier	22	A	No	No
			B	No	No
17	Staffordshire Bull Terrier	36.4	A	Osteophytosis, enthesophytosis and subtrochlear sclerosis	Yes
			B	Osteophytosis, enthesophytosis and subtrochlear sclerosis	Yes
18	Border Collie	19.8	A	No	No
			B	No	No
19	Shih Tzu cross	19	A	Palpable disease prior to radiography	Yes
			B	Palpable disease prior to radiography	Yes
20	Great Dane	48.3	A	Palpable disease prior to radiography	Yes
			B	Palpable disease prior to radiography	Yes
21	German Shepherd Dog	23.6	A	No	No
			B	No	No
22	Siberian Husky	22.8	A	No	No
			B	No	No
23	Jack Russel Terrier	11.7	A	Palpable disease prior to radiography	Yes
			B	Palpable disease prior to radiography	Yes
24	Terrier cross breed	6.1	A	Incongruence	Yes
			B	No	Yes
25	Shetland Sheepdog	5	A	Enthesophytosis, mild incongruence	Yes
			B	Enthesophytosis, mild incongruence	Yes
26	Terrier cross breed	6.7	A	Elbow incongruence	Yes
			B	Elbow incongruence	Yes

Table 2.3.1: Table listing cadaver selection and exclusion based on criteria described in Section 2.1 and 2.3.

Examples of Radiographic Projections from Specimens Included in the Study

Figure 2.3.1: Radiographic projections obtained of identifier 16 included in the study.

Examples of Specimens Excluded from the Study

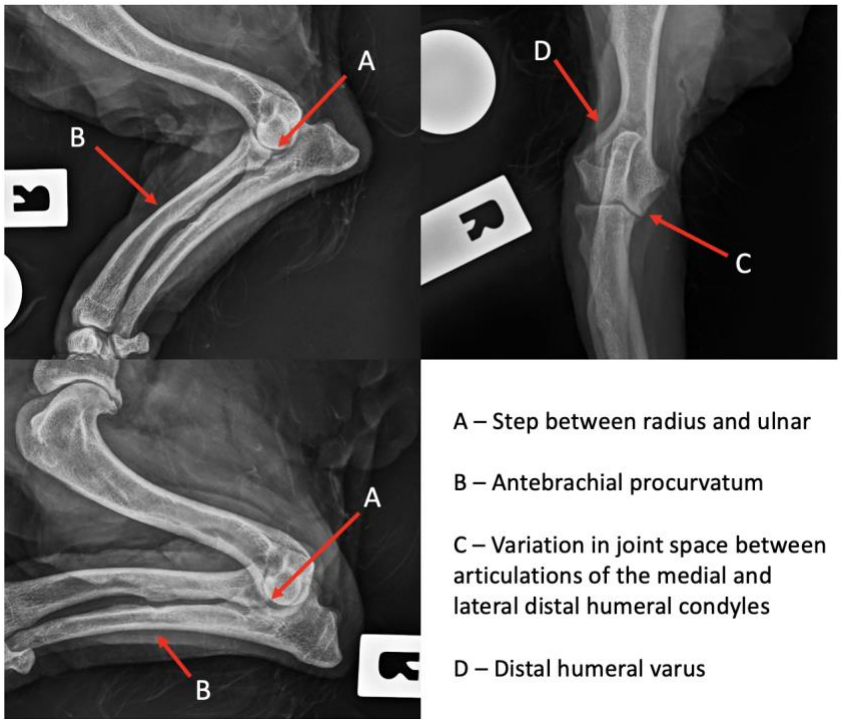

Figure 2.1.2: A selection of radiographic projections obtained from identifier 26A excluded in the study. Top left: mediolateral neutral projection. Top right: craniocaudal projection. Bottom left: mediolateral flexed projection. Bottom right: key to annotations identifying specific pathology.

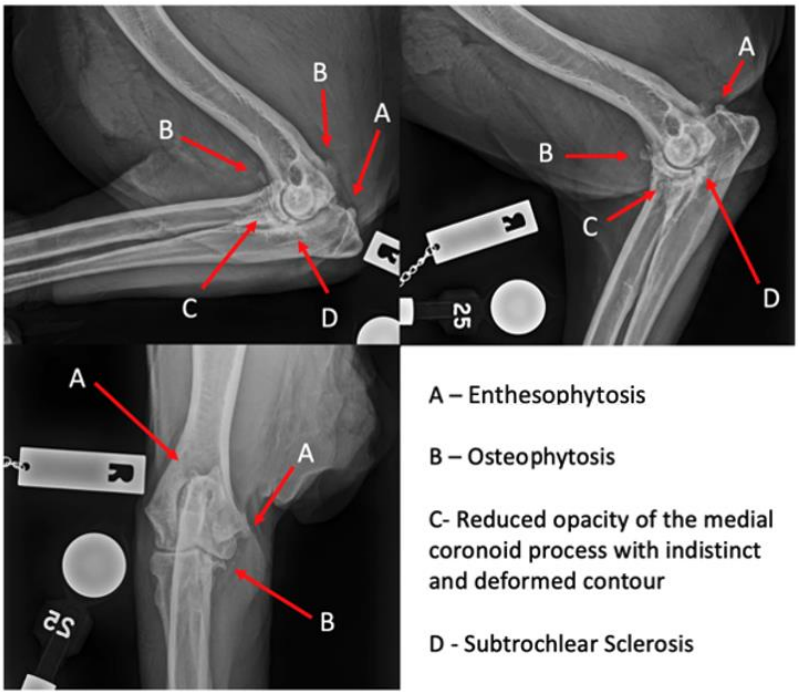

Figure 2.3.3: A selection of radiographic projections obtained from identifier 17A excluded in the study. Top left: mediolateral flexed projection. Top right: mediolateral neutral projection. Bottom left: craniocaudal projection. Bottom right: key to annotations identifying specific pathology.

During specimen preparation, intraarticular structures were examined for gross evidence of pathology such as cartilage erosion, incongruency, osteophytosis or chondromalacia by palpation of the cartilage. Detection of intra-articular pathology resulted in exclusion from the study. Examples of limbs where intra-articular pathology was detected are shown in Figure 2.3.4.

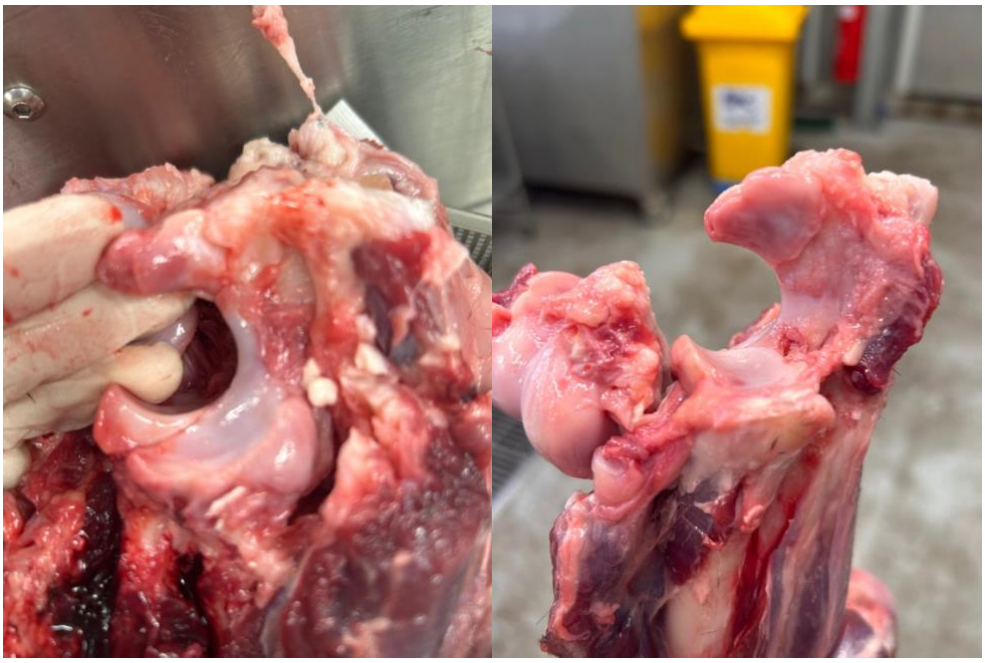

Figure 2.3.2: Photographs of the intra-articular surface of specimen 11 B. Upon gross examination of the joint osteophytosis and an ununited anconeal process were observed as well as ulceration of the cartilage within the cranial aspect of the medial compartment and mild radioulnar incongruence.

2.4 Specimen Preparation

Skin and subcutaneous tissues were removed to the level of the mid-antebrachium and tissues proximal to the humerus were discarded after disarticulation at the glenohumeral joint. Proximal to the elbow joint, fascia, muscle and neurovascular structures were removed preserving the origins of the antebrachial muscles and collateral ligaments. The extensor carpi radialis muscle dissected off the insertion on the distal radius and reflected distally to allow access to the elbow joint medially. A 4.0mm drill bit was used to create a transcondylar bone tunnel through the distal humerus. A medial epicondylar osteotomy was then performed with a sagittal oscillating bone saw without damage of the articular cartilage. Where necessary to allow evaluation and access of the elbow joint, joint capsule and pericapsular far was dissected with care to preserve the myotendinous units, LCL and MCL and annular ligament.

The medial epicondyle was anatomically reduced with point to point bone holding forceps and secured with a 3.8mm transcondylar bolt and wing nut.

The LCL was exposed by transection of the lateral digital extensor and ulnaris lateralis muscle bellies with Mayo scissors which were reflected proximally.

Figure 2.4.1: Lateral view of cadaveric specimen showing the cranial crus (blue star) and caudal crus (green star) of the LCL.

2.5 Specimen Storage

Specimens were then wrapped in laparotomy sponges soaked in 0.9% NaCl and double bagged. They were stored at -20ºC and thawed as previously described prior to testing.

Chapter 3:

Experimental Design

3.1 Selecting and Obtaining a Data Acquisition System

Pressure is measured in terms of force acting on a known area with the standard international unit of Pascals or Newton's per square meter (56). Force is defined as an influence that can change the velocity of an object by the equation F (force of magnitude) = M (body of mass) x A (acceleration) and is measured in Newtons (57). The purpose of this chapter is to describe the process of finding an appropriate sensor and data acquisition system to measure and record, in real time, the force, pressure and distribution within the canine elbow in axial loading under different experimental conditions.

Measurement of joint surface kinematics in the veterinary literature utilizes polymethyl methacrylate casting, the finite element method, fiduciary arrays and tactile array sensors (58–62). The ideal data acquisition system will allow for continuous, real time recording and not require manipulation between experimental conditions to ensure consistency of measurements. The acquisition system must be validated for intra-articular use and able to transmit data to a readily available computer system for data analysis. Tactile sensors fulfil these requirements.

Tactile sensors are data acquisition devices used to measure tactile-related properties through direct physical contact (63). Three typical principles of transduction that tactile sensors are based on are (1) capacitance, (2) piezoresistivity and (3) piezoelectricity. Sensor type selection can be guided by considering the application of the sensor. A piezoresistive sensor is composed of a pressure sensitive element whose resistance varies when force is applied (64). When combined with a conductive polymer, external electrical activity is transduced to generate tactile data – V (voltage) = I (current) x R (resistance) (64). Tactile pressure sensors are designed by arranging the transduction and conductive polymers in a known configuration to measure force and thus pressure by way of force mapping. A diagrammatic representation is shown in Figure 3.1.1. Additionally, this allows measurement not only of direct force and pressure but also peak forces and pressures in real time (56,57,64).

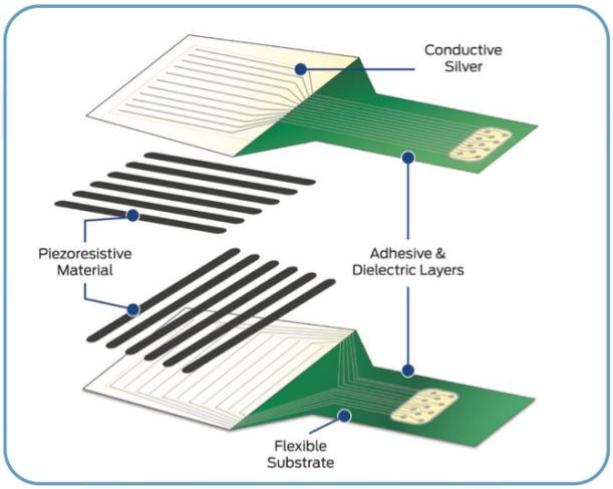

Figure 3.1.1: Diagram showing components of a tactile array sensor (TekScan)

In the veterinary literature, elbow contact mechanics have been investigated with tactile sensor systems by companies including novel.de and Tekscan (26,33,58,62). Through collaboration with researchers at an external laboratory, the Surgery and Orthopaedics Research Laboratory (SORL), training and access to the I-Scan system by Tekscan was provided. The I-Scan system uses a thin, flexible sensor to measure interface pressure between two surfaces. The system is comprised of a sensor which transmits information through 'Evolution', the data acquisition electronics, to a computer via a USB port.

Tekscan matrix-based sensors are less than 0.1mm thick making them appropriate for intra-articular placement. Tekscan produces commercially available sensors by catalogue order as well as custom designed sensors. Sensor selection from the catalogue was deemed most appropriate to maximise both time and financial resources. Sensors needed to be chosen based on size and resolution. Resolution refers to the number of sensels per centimetre squared. A sensel is the term used to describe the intersection of the horizontal and vertical piezoresistive material creating a grid pattern of sensels. Optimal sensor selection will analyse the entire intra-articular surface area simultaneously at the highest resolution possible to allow for mapping of specific regions within the joint.

Sensor selection for the final experimental model involved consideration of four sensor types and experimental trials with five of these. Sensors considered and trialed are shown in Table 3.1.1. Sensor 6900 was tested in the first stages of the experimental design stage, this was a recycled sensor donated by SORL laboratory. The sensor design of four legs allowed in sensor placement in both the medial and lateral compartment with simultaneous data acquisition of both compartments during experimental testing. This design would allow for use of two sensor pads per experiment, preserving the remaining two for later testing. Prior to sensor placement, sensors must be tested and calibrated to ensure accuracy. During the testing phase of sensor 6900, it was found that two of the sensor pads had defects resulting in sensel loss. The conductive silver lies within the flexible substrate which results in the thin and flexible design. The flexible substrate has properties similar to that of a thin plastic sheet. As a result, plastic deformation during prior experiments with this sensor occurred interrupting single transduction from the sensel to the data acquisition electronics resulting in regions of data 'dark space'. This was the first occurrence during experimental testing of sensor damage, damaged sensors were discarded.

The testing of sensor 6900 allowed establishment of an experimental model however due to limited availability of recycled sensors at SORL, additional sensors needed to be purchased. This allowed for consideration of other sensor types. Sensors 4205 and 5800 were considered however design limitations would only allow for placement in one compartment. Movement of the sensor during the experiment would potentially lead to variations in placement during data acquisition and loss of accuracy in pressure and force mapping. Sensor 4205 was of an appropriate size to sit within the joint and span both the medial and lateral compartment however plastic deformation occurred as noted with sensor 6900 causing irreversible damage to the sensor. Additionally, based on results of similar experiments, these sensors may not have the capacity to measure maximum intra-articular pressures during maximum axial loading (33,58,62). Sensors 4000 and 4041 were therefore considered more appropriate. Sensor 4000 was available as a recycled sensor from SORL and although this sensor has cuttable tabs to facilitate placement, the matrix width resulted in overlapping of the sensors axially which initially was preferable as this allowed superimposition of data acquired by each matrix facilitating intra-articular mapping. During loading, the axial overlap and lateral protrusion of the sensors medially and laterally beyond the joint contact area resulted in plastic deformation

and sensor damage. Sensor 4041 was therefore considered the best commercially available option. Bilby Shoes imports and provides support Tekscan products in Australia. The company was contacted in November 2022 to place an order for sensors 4041, delivery of the sensors from America was in July 2023.

Model	Image	Matrix Width	Matrix Height	Resolution	Maximum pressure (kPa)
4000	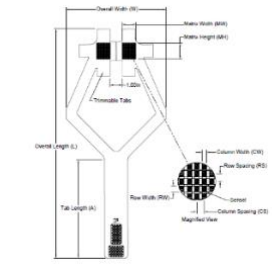	27.9	33.0	62.0	10,342
4041	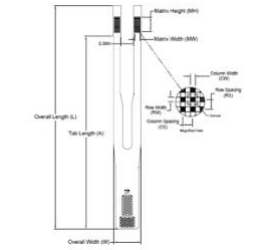	12.7	31.5	22.8	13,790
4205	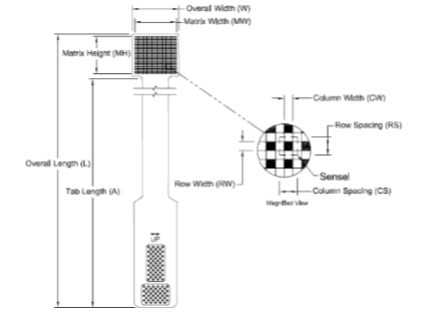	45.7	41.9	27.6	2,068
5800	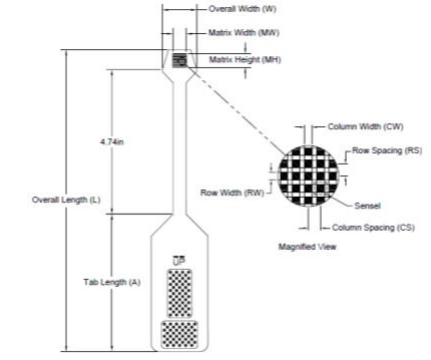	12.7	12.7	62.0	248

6900	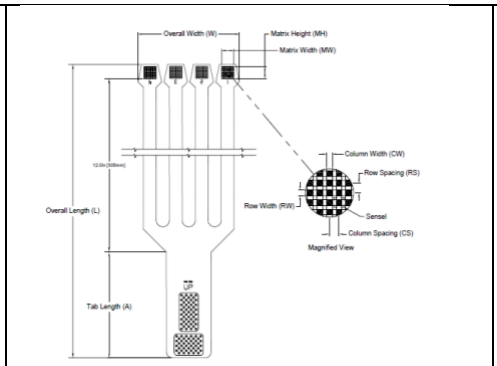	14.0	14.0	62.0	68,948

Table 3.1.1: Table showing TekScan sensor characteristics considered for use in this study.

3.2 Experimental Set Up Design

Development of a suitable testing jig for the experiment required three components. The limb needed to be secured proximally with the ability to rotate 350 degrees mimicking the glenohumeral joint whilst the base of the pes was kept immobile but non-constrained. Due to the excision of soft tissues proximal to the elbow joint, the triceps mechanism needed to be constructed and allowed to mimic shortening and lengthening of the muscles resulting in variable extension and flexion of the elbow joint. This testing jig would need to be suitable for placement on a materials testing system (MTS) for limb loading and simulation of forces applied to a normal limb during ambulation.

3.3 Simulation of the Triceps Brachii Myotendinous Unit

The triceps brachii muscle is comprised of four heads, three of which originate from the proximal humerus and one from the scapula. All four heads insert on the olecranon (65). Together, the triceps brachii myotendinous unit functions to flex the shoulder and extend the elbow joint. After dissection of the soft tissues proximal to the elbow, it was therefore necessary to simulate the triceps brachii myotendinous unit due to its function in supporting body weight and ambulation.

This mechanism was tested to ensure functionality by creating a system to hold the limb in a standing position whereby the simulated triceps brachii myotendinous unit could be adjusted to flex and extend the elbow during axial loading of the limb. A 50 x 60cm perforated aluminium sheet was suspended at four points by multifilament polyester line to create the 'celling' of the system. This was buttressed with additional steel plates secured with screws and nuts to prevent bending of the construct. The PVC cup was secured to the metal plates via the perforations with a threaded stainless steel O-ring and nut. Aeroplane wire was passed through a bone tunnel in the olecranon and secured with a wire rope grip to create a loop. This loop was secured to another loop of aeroplane wire with a 6mm stainless steel swivel to allow for 360 degree motion of the construct. This most proximal loop was secured with another wire rope grip with one of the tails of aeroplane wire passing proximally to traverse along the celling of the construct before changing course distally to be anchored at the level of the antebrachium. Lengthening and shortening of the aeroplane wire simulated triceps brachii muscle contraction and extension

During this trial period, different equipment and configurations were trialed to reduce friction of the aeroplane wire with the construct and best simulate the direction of force of triceps brachii muscle contraction.

Design 1

The first design, shown in Figure 3.3.1, utilized pulleys and hooks secured either end of the celling construct with the aeroplane wire passing lateral to the PCV cup through a central O-ring on the underside of the celling construct. During simulated muscle contraction, due to the non-constrained pulleys, the working length of the contraction reduced in the early stages of contraction without elbow extension. This inconsistent tension on the simulation resulted in unpredictable degrees of elbow flexion and extension. In addition to this, the leader line traversing lateral to the PCV cup resulted in friction with the cup as well as a lateral force resulting in unwanted rotation of the limb.

Figure 3.3.1: Photographs of experimental set up of design 1

Design 2

To address the inconsistent tension during simulated contraction, the pulleys were replaced with O-rings secured in place of the hook and pulley at either end of the celling construct. The central O-ring was further lateralised to prevent friction of the aeroplane wire with the PCV cap. It was hypothesized even with further lateralisation of the central O-ring, rotation of the elbow would be minimised by creating a negating vector of pull between the central O-ring and the turning point of the aeroplane wire before distal attachment to the table. Upon simulation of the triceps brachii muscle contraction, elbow rotation was still evident and suspected to be caused by friction points in the construct, this can be seen in Figure 3.3.2.

Figure 3.3.2: Photographs of experimental set up of design 2

Design 3

Elbow rotation was addressed by traversing the aeroplane wire over the ceiling the construction in order to better mimic the direction of pull of the triceps brachii muscle. Construct design was simplified by using fenestrations in the metal sheets for leading of the aeroplane wire. There was concern the interface between the fenestration and the aeroplane wire would cause inconsistent friction and thus tension in the construct however this was not the case during simulation of triceps brachii muscle contraction.

Design 3, shown in Figure 3.3.3, allowed proof of concept to simulate the triceps brachii muscle during axial loading of the limb. During this phase of the experimental design, access to the materials testing system had not yet been made available. It was later evident that a more simple and compact design would be required so ensure compatibility with the materials testing machine.

Figure 3.3.3: Photographs of experimental set up of design 3

Design 4: The final design

The final design utilized an adjustable turnbuckle secured to the proximal humerus and olecranon at the points of origin and insertion of the triceps brachii muscle. This design allowed easy adjustment of the degree of flexion or extension of the elbow in a compact construct which was compatible with the materials testing machine. This design would also allow replication of the construct in future studies where the flexion angle of the elbow may be adjusted.

Final preparation of the triceps brachii unit, shown in Figure 3.3.4, was as follows: a 4.0mm drill bit was used to drill a hole in the proximal humerus, caudodistally at the level of the neck to cranioproximally to exit medial to the lateral tuberosity. The tunnel was placed to align with the anatomical position of the triceps brachii myotendinous unit attaching distally at the olecranon. A 3.5mm drill bit was used to create a bone tunnel through the olecranon. The tunnel was started cranial to the bursa where the triceps brachii was previously removed to caudally approximately 1.5cm distal to the top of the bone to exit. A 3.8mm and 3.2mm O-ring screw and wing nut were placed in each bone tunnel respectively to anchor the turnbuckle.

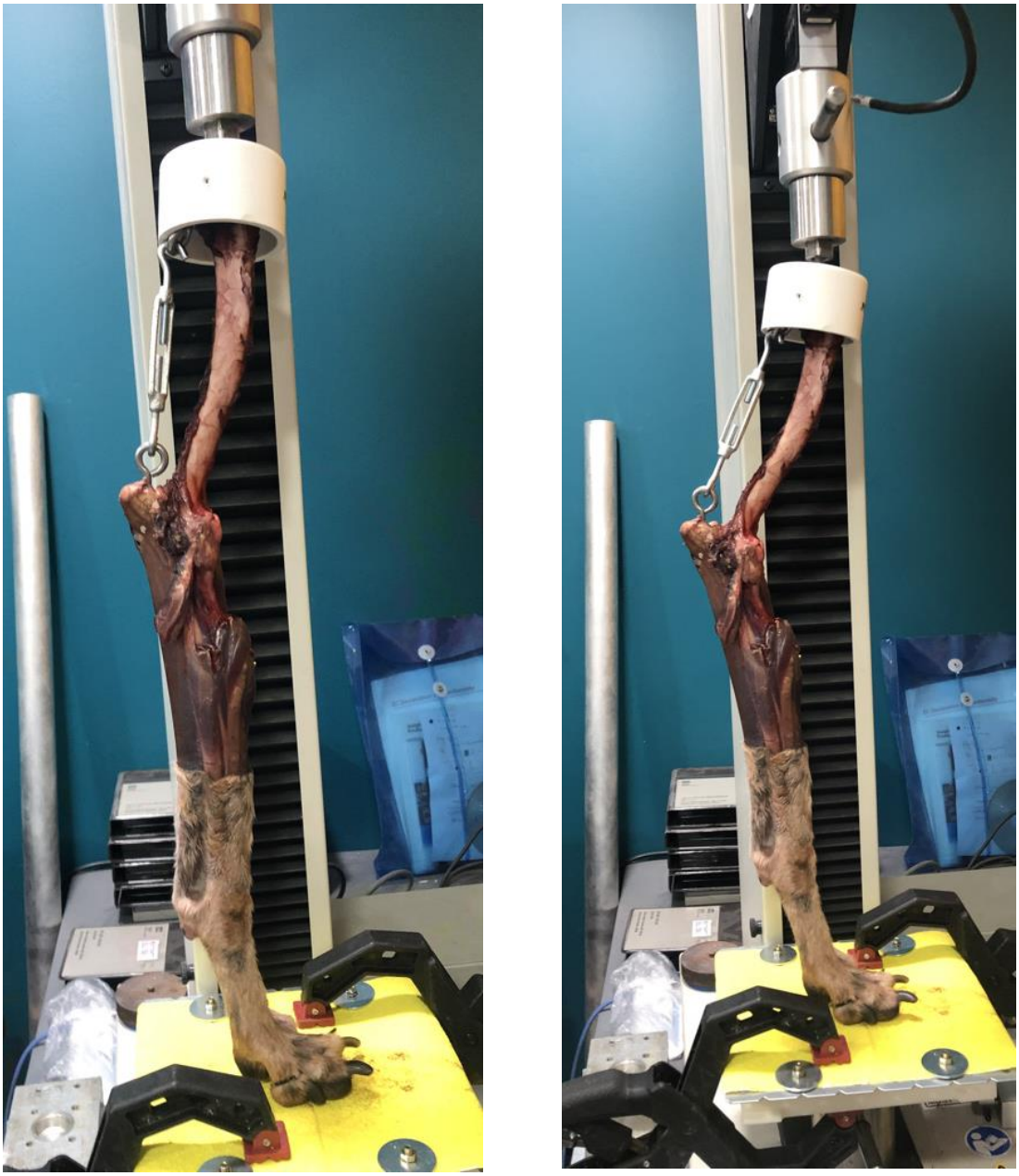

Figure 3.3.4: Photograph of limb mounted on materials testing machine.

3.4 Materials Testing System

Materials testing Systems (MTSs) are used to measure force and displacement during compression, shearing, bending or stretching of the test material, in this case, the limb. A MTS is composed of a load bar which is electronically controlled via computer software to move upwards and downwards applying axial load. The same software can control the magnitude of the applied axial load by use of a load cell. The load cell measures and records vertical force data and is positioned under the experimental sample. Load bar round nuts are used to secure samples or accessories to the load bar for testing. Development of the testing jig required a set up that was compatible with this system. Press PCV cap ends were sourced from a local hardware store. The shape allowed for placement of the proximal humerus within the cap which

could be secured to the load bar with a load bar round nut. The press PVC cap allowed for proximal security of the limb whilst simulating the range of movement of the glenohumeral joint during axial loading. Distally, a metal plate covered with coarse sandpaper was secured to the load cell with spring clamps. This design allowed for the replacement of the sandpaper between experiments to reduce bacterial contamination of the experimental design and ensure consistency between experiments.

The final experimental set up allowed for controlled application of axial force on a non-constrained canine thoracic limb. Continuous and simultaneous data were collected electronically by computer software for each experimental condition without the requirement to manipulate the limb placement on the MTS or the sensors within the joint.

Data obtained from the MTS during experimental trial runs showed consistent, predictable and repeatable crosshead movement indicating the final experimental design was stable and not transformed between experimental runs giving confidence in repeatability between experimental conditions. This is shown in Figure 3.4.1, a still shot obtained from the MTS system during experimentation with height on the x-axis and load (N) on the y-axis.

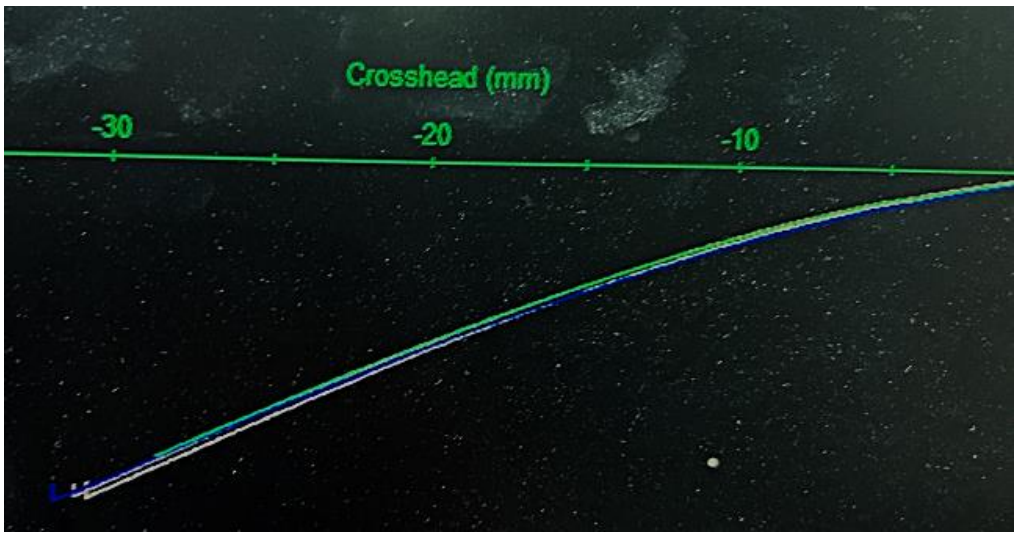

Figure 3.4.1: Still frame obtained from MTS electronic data acquisition system during experimentation. X-axis = crosshead height (mm), Y-axis = loading force (N).

Chapter 4: Refinement of Experimental Technique

4.1 Developing the Methodology

4.1.1 Introduction and Objective

The objective of this study was to evaluate the contribution of the LCL on the biomechanics of the canine elbow joint. It was hypothesised that by placing Tekscan sensors within the medial and lateral compartments of the elbow, changes in force distribution could be compared between experimental conditions. In the early experimental phase of the study, the methodology was refined in order to ensure:

1. TekScan sensors could be placed within the medial and lateral compartments of the canine elbow joint.
2. Experimental set up allowed changing of experimental conditions without modifying the placement of the TekScan sensors within the joint.
3. Data obtained was accurate and repeatable.

The purpose of this chapter is to describe the experimental technique and discuss the challenges and solutions which were encountered during this process.

4.1.2 Method

The thoracic limbs were prepared as described in Chapter 2. The medial and lateral compartments of the elbow were accessed by removing the 3.8mm transcondylar bolt and wing nut to retract the medial humeral epicondyle and expose the intra-articular surfaces. Tekscan sensors (model 4041) were placed in the medial or lateral compartments and digitally secured in place while the medial humeral epicondyle was reduced, compressed and the transcondylar bolt and wing nut was used to secure the construct.

Challenge 1: Accurate placement of the sensors so the sensel containing region was within the medial and lateral compartments was obstructed by soft tissues at the caudal aspect of the joint.

Solution 1: Further dissection of the soft tissues on the caudal aspect was required to allow protrusion of the non-sensel region of the sensors from the caudal aspect of the joint. This placement has been described in similar studies however was initially opted against in order to retain as much normal anatomy as possible to better simulate a normal elbow (66,67). During the early phases of the experimental period, it was deemed necessary to have the sensors protruding through the caudal aspect of the joint to avoid sensor migration during reduction of the fracture fragments. This also allowed monitoring of the length of sensors protruding caudally during the experiment to ensure the sensors were not migrating during testing.

Challenge 2: Reduction of the fracture fragments whilst ensuring correct placement of the Tekscan sensors was challenging without an assistant. In addition, once the fracture fragments were reduced during the process of compressing the osteotomy, the medial humeral epicondyle rotated as the transcondylar bolt was tightened resulting in an intra-articular step. Some investigators have described securing the sensors to the tissue with screws, glue or a combination of these through the outer plastic of the sensors (22,66,67). This was not considered due to the potential damage caused to the sensors. Strategies used to overcome this

included utilising a tabletop vise to aid in immobilisation of the limb, placing an additional smaller 1.5mm cortical screw through the proximal aspect of the fracture fragments, using an anti-rotational k-wire and compressing the osteotomy with point-to-point bone holding forceps.

Solution 2: Immobilisation of the limb with a tabletop vise and the use of point-to-point bone holding forceps allowed for one operator to ensure correct placement of the sensors, accurate fragment reduction and stabilisation of the fracture fragments with bone holding forceps. Some specimens required the placement of two sets of point-to-point bone holding forceps to prevent rotation of the medial humeral epicondyle during tightening of the transcondylar bolt.

The distal humeral articular surface was visually evaluated to ensure perfect reduction of the distal humeral epicondylar osteotomy. The limb was placed onto the materials testing system as described in Chapter 3.

Challenge 3: The PCV pipe cap was not able to be rigidly secured to the materials testing system due to limitations with available equipment at the laboratory.

Solution 3: The PCV pipe cap was substituted with a metal cup with a smooth inner surface, shown in Figure 4.1 below. This metal cup had been previously custom designed for the materials testing system to ensure compatibility. This provided the same function as the PCV cup but was more rigidly secured.

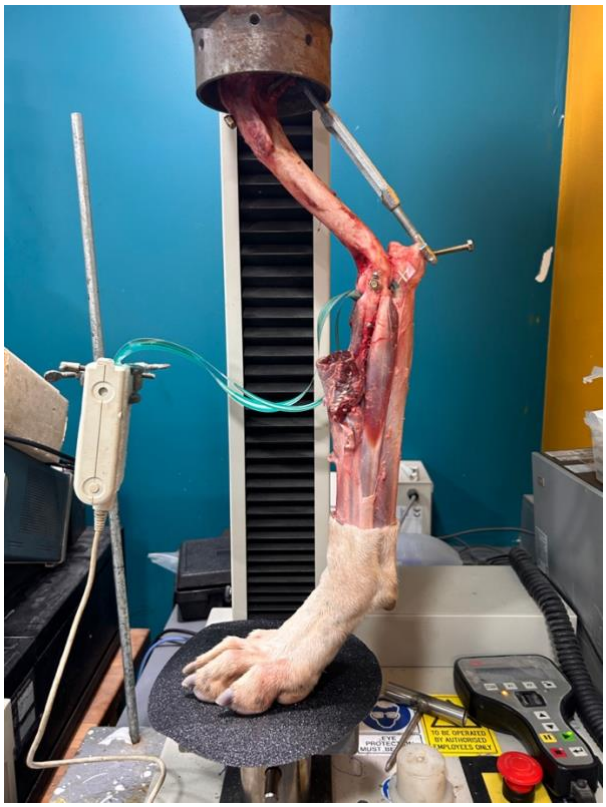

Figure 4.1.1: Alternate experimental set up with PCV cup replaced with metal cup.

The sensor was loaded into the data acquisition electronics which was secured on a retort stand to allow for movement of the limb on the materials testing system without tension on the sensors which would result in sensor movement.

The limb was pre-loaded to 50 N to maintain stability of the limb during experimental set up. A goniometer was used to ensure an elbow angle of 135 degrees by adjustment of the turnbuckle.

Challenge 4: Initially, we aimed to evaluate the effect of three different elbow angles to simulate the elbow in extension, neutral and flexion. The inclusion of different elbow angles resulted in an additional twelve experimental conditions which were each ran in triplicate i.e., 36 experimental runs per specimen. The time required to complete each specimen limited the number of specimens that were able to be assessed. There was an additional concern that with repeated loading, soft tissue deformation may occur which could compromise the accuracy of the data.

Solution 4: One elbow angle of 135 degrees was tested based on the normal standing angle of a racing greyhound (34,68). This resulted in 4 testing conditions and twelve runs per specimen which was achievable considering the time required for experimental set up and testing.

Four conditions were tested three times with each loading to 200 N and holding at that load for 30 seconds. Testing conditions included: intact (1), cranial or caudal crus of the LCL transected (2), LCL transected (3), and prosthetic LCL placed (4).

1. Intact

The experiment was repeated three times with the limb placed as previously described.

2. One crus of the LCL was transected, either the cranial or caudal crus.

The selection was made based on a coin toss iPhone application as to which crus was incised. For subsequent experimentations this would be performed on the first experiment and alternated for each experiment thereafter. Access to the LCL was previously ensured during cadaver processing as described in Chapter 2.2.4. The selected crus was completely transected with a size 11 scalpel blade and Adson thumb forceps without disturbance of any other component of the experimental set up, shown below in Figure 4.1.2.

Figure 4.1.2: Lateral view of the elbow during testing, mounted on the MTS. Adson tissue forceps indicate where the cranial crus of the lateral collateral ligament has been transected.

3. Entire LCL was transected.

The remaining crus was transected with the same technique as used for the previously transected crus resulting in a LCL defective elbow joint. This is displayed below in Figure 4.1.3.

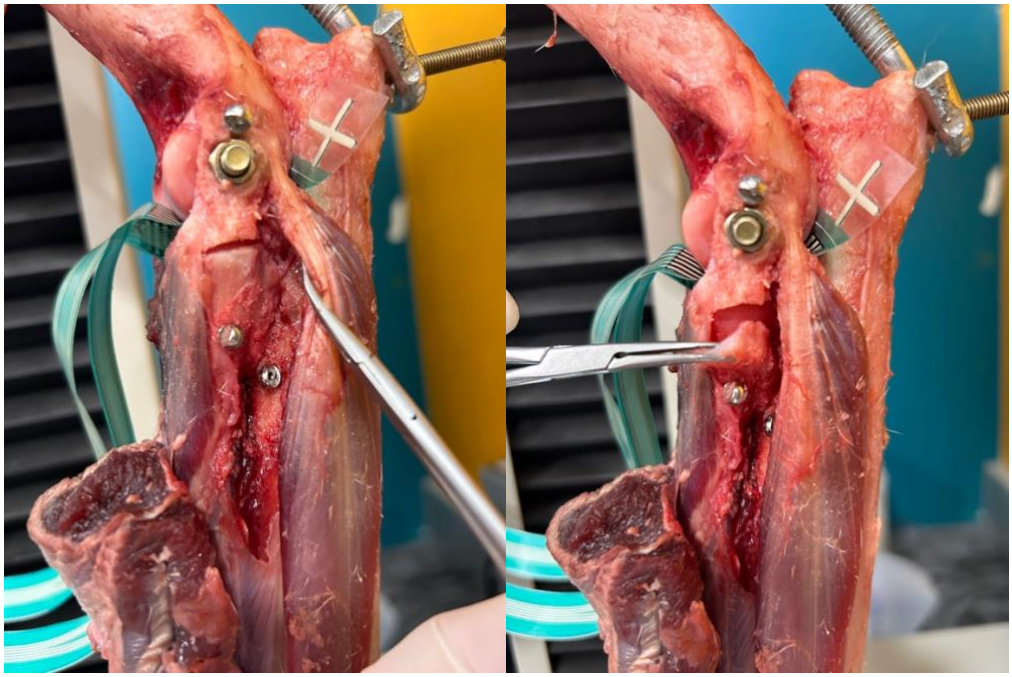

Figure 4.1.3: Lateral view of the elbow during testing, mounted on the MTS. On the left, mosquito haemostats are reflecting the soft tissues to reveal the entire lateral collateral

ligament. In the image on the right, the mosquito haemostats are demonstrating transection of the entire lateral collateral ligament.

4. Placement of a prosthetic LCL.

Polypropylene monofilament suture (1 Prolene, Ethicon) was secured to previously placed suture anchors described in Chapter 3.2. Placement was based on mimicking the cranial and caudal crus of the LCL and secured with a surgeon's knot with six throws under tension. An example of placement is shown below in Figure 4.1.4.

Figure 4.1.4: Lateral view of the elbow during testing, mounted on the MTS showing placement of the prosthetic lateral collateral ligament.

4.2 Cadaveric Specimen Exclusion

Fifty-one canine thoracic limbs from twenty-six canine cadavers were evaluated for the experiment. Of these, thirty-two limbs were excluded due to the presence of elbow pathology detected radiographically or by gross visual inspection of the intra-articular surfaces. Of the nineteen thoracic limbs where elbow pathology was not detected, two of these were excluded due to the size of the joint. These limbs were from a 12 kg chihuahua where the sensors could not be placed accurately within the joint to overlay either the medial or lateral compartment. During refinement of the experimental method described above, two limbs were unable to be used for the experiment and were discarded after damage to the specimen during problem solving for *challenge 1 and 2*. Data were collected on seven thoracic limbs. The remaining eight limbs which had been screened and prepared for experimental testing were disposed due to concerns with tissue degradation which would change tissue properties affecting experimental results. Specimens were intended for experimentation however due to the

requirement to refine the experimental technique as described earlier in this chapter, these specimens progressively deteriorated and were no longer considered viable for this experiment. Repeated thawing and freezing of cadaveric specimens is not recommended to maintain mechanical properties of the cadavers and prevent colonisation of bacteria for health and safety purposes (69). Figure 4.2.1 summarises the outcome of limbs intended for use in this study which is detailed in Table 2.3.1.

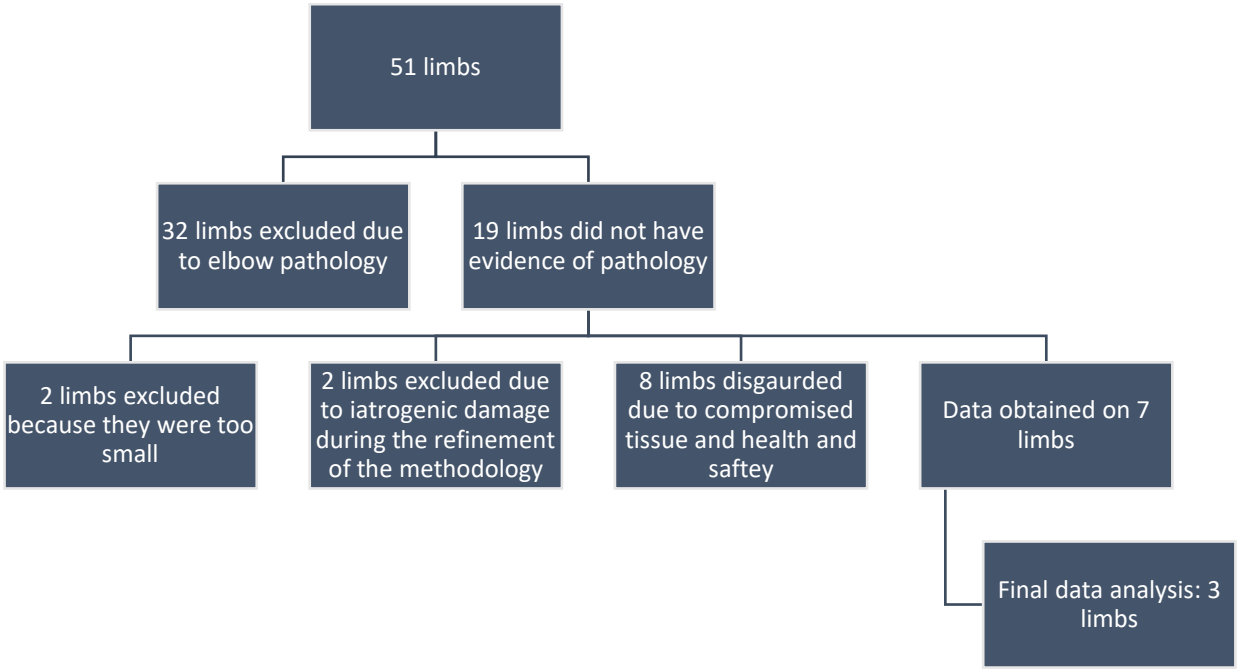

Figure 4.2.1: Flow diagram summarising the use of cadavers for this study.

Cadaveric Specimens Which Underwent Experimental Testing

Seven canine thoracic limbs underwent experimental testing, of which 3 were included in the final data analysis. These included: specimen 1 a Staffordshire Bull Terrier of 29.1 kg, specimen 2 a Siberian Husky of 24.3 kg and specimen 3 a Greyhound of 28.4 kg. These were selected for consistent pre-load forces of 40–50 N and absence of sensor artefacts. Of the limbs which were tested but not included in the final data analysis, data were collected for 3 limbs.

Prior to each experimental testing session for each limb, limbs were pre-loaded 40-50N to allow proper positioning of the limb and apparatus. Data were recorded for each experimental session at time 0. This corresponded to the 'pre-loading' phase of the experiment. Data acquired from all seven limbs is displayed in Table 4.2.1 below.

	S 1	**S 2**	**S 3**	**S 4**	**S 5**	**S 6**	**S 7**
Intact	47.9	42.3	46.5	856	41.6	141.3	5.0
One crus cut	46.9	45.3	43.1	856	4.1	136.6	1.7
Both LCL crura cut	41.7	43.4	22.6	856	17.0	136.2	0.7
Prosthetic ligament placed	52.4	47.8	30.3	856	33.5	135.1	3.0

Table 4.2.1: Table showing force (N) acquired during experimentation on the 7 limbs where data were obtained. Red = excluded due to exceedingly high readings. Blue = excluded due to exceedingly low readings. S = specimen

During data quality control, four of the seven limbs which underwent experimental testing were excluded from final analysis: specimens 4-7. In specimens 4 and 6, sensor deformation yielded high baseline forces of 856 N and 135–141 N respectively, versus the expected pre-load of approximately 40-50 N. Inadvertent sensor displacement during LCL transection occurred in specimen 5, with an unexpected low force of 4.1 N post-transection of one crus. Specimen 7 measured consistently low forces of <5 N across conditions, indicating incomplete sensor placement. These are summarised in figure 4.2.1 and table 5.3.

Force data acquired within the joint during loading does not equal the force applied by the materials testing machine. The transmission of force through the limb is not isolated through the joint, but the limb as a whole. In addition, anatomical variation including muscle mass, age of the dog and variations in the biomechanical properties of the tissues result in variations between specimens.

One limitation of this experiment was access to uniform cadavers and standardisation of experimental conditions. Less variation between cadavers and consistent time since death, time frozen, defrosting conditions and time, room ambient temperature, etc. would have likely reduced variability between specimens. There is no guideline for accepted variability published in the literature, however specimens 4 and specimen 6 produced forces higher than anticipated at time 0. Upon evaluation of the sensors at the conclusion of the experiment, the plastic covering was deformed secondary to damage obtained during the experiment or in storage. Deformation of the plastic compresses the sensors creating a force reading which is not reflective of the intra-articular conditions, rather the conditions within the sensor. For this reason, specimens 4 and specimen 6 were excluded.

Specimen 5 and specimen 7 were excluded due to the positioning of the sensors. While adjusting experimental conditions to cut the cranial crus of specimen 5, the sensors were inadvertently disturbed. This can be viewed in Table 4.2.1 above where the average force at time 0 for the second experimental condition is markedly lower than expected. This is suspected to be due to the sensors being repositioned elsewhere and thus measuring data unrelated to the experimental aims. Similarly, the sensors for specimen 7 were placed incompletely within the medial and lateral joint compartments. Specimen 5 was obtained from a young adult Staffordshire bull terrier with good muscling, this resulted in more extensive dissection in order to place the sensors. When processing this specimen, care was taken to dissect the minimum in order to best simulate the biomechanics of a live dog. This approach resulted in difficulty placing the sensors for this specimen.

4.3 Statistical Testing

Statistical analysis was performed with a statistical package program, GenStat version 22. Statistics were conducted on a proportion measure for each of the 5 outcomes: Force, Area, Pressure, Peak Force and Peak Pressure. This proportion was calculated by dividing the individual lateral value by the whole joint value for each outcome to produce a proportion of the whole. These proportions were then deducted from the baseline (whole joint; no treatment) to obtain an estimate of change from the baseline. A linear model statistical test was utilised to assess the effect of treatment in each experimental condition on the change in proportion from the baseline for each of the outcomes. A P value of < 0.05 was considered statistically significant.

Statistical analysis was performed using GenStat version 22. Five outcomes were analysed: force, contact area, pressure, peak force, and peak pressure. For each, a proportion was calculated as (lateral compartment value / whole joint value), then subtracted from the intact baseline to estimate change. Due to the paired, self-controlled design with each specimen serving as its own control across conditions, a linear mixed-effects model was fitted with treatment (half-cut, full-cut, prosthetic) as fixed effect and specimen as random effect, assessing change from baseline. Parametric assumptions were not formally tested; data were not transformed due to small sample size. $P<0.05$ was considered significant.

Limitations of this approach include low degrees of freedom (df=2 for n=3), risking overfitting in linear models and inflated Type I error. An equivalent one-sample t-test against zero change (or repeated-measures ANOVA on proportions) may have been more robust for this paired design, but linear modelling was selected for its flexibility with proportions. Results should be interpreted cautiously as exploratory, not confirmatory.

No formal a priori power analysis was performed due to the exploratory nature of this ex vivo cadaveric study and logistical constraints on specimen availability. Post-hoc power calculations for the primary outcomes (force and pressure proportions) using observed effect sizes, Cohen's d approximately 0.8–1.2, $\alpha=0.05$, and n=3 per condition yielded power of 0.45–0.62. This indicates underpowering for detecting medium-to-large effects. Larger sample number of 8–10 per group would be required for >80% power based on similar biomechanical studies (70,71). The resultant small sample size reflects the final analysable specimens after rigorous exclusions, prioritising data quality over quantity.

Chapter 5: Results

Full transection of the LCL in the canine forelimb cadavers increased both the force and contact pressure within the medial compartment of the canine elbow. When analysed as a proportion of whole-joint values, full transection of the LCL increased medial compartment force by 6.33 ±1.49 N; P=0.023 and pressure by 5.80 ±1.46 kPa; P=0.045. Contact area did not show a significant change and placement of a prosthetic LCL did not restore normal intra-articular joint contact mechanics. P-values obtained are exploratory and should be interpreted cautiously due to the small sample size used in the final data analysis. These results are shown in Table 5.1 and Figure 5.1 below.

	Half Cut		Full Cut		Prosthetic	
Parameter	Δ	%Δ	Δ	%Δ	Δ	%Δ
Force (N)	1.072	+1.6%	6.33	-9.0%	-1.485	-2.2%
Area (mm^2)	-0.2389	-0.3%	0.7729	+1.0%	-0.7813	-1.0%
Pressure (kPa)	1.303	+1.2%	5.798	-8.7%	-1.46	-2.2%
Peak Force (N)	1.304	+1.9%	4.729	-7.2%	-1.182	-1.8%
Peak Pressure (kPa)	1.296	+1.9%	4.723	-7.1%	-1.183	-1.8%

Table 5.1: Absolute changes (Δ) and percentage changes (%Δ) in contact mechanics parameters for the lateral compartment as a proportion of the whole joint under different testing conditions. Positive Δ values indicate an increase in the lateral proportion (decrease in medial proportion) relative to the intact baseline; negative values indicate a decrease in lateral proportion (increase in medial proportion).

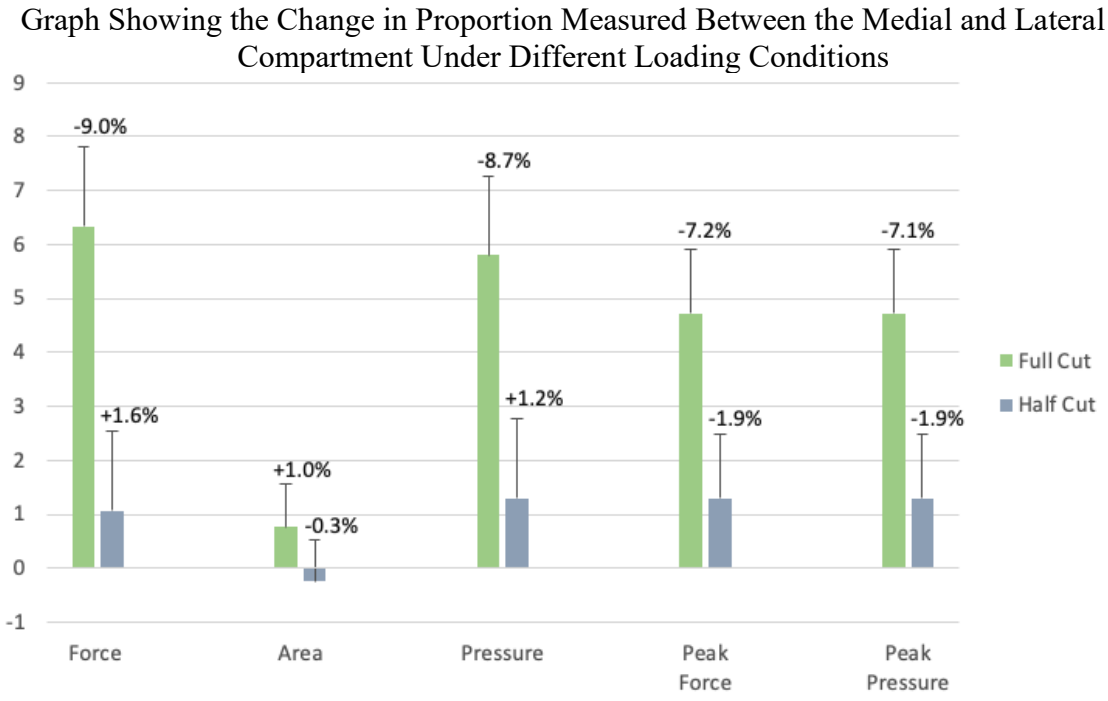

Figure 5.1: Visual representation of absolute changes (Δ; bars) and percentage changes (%Δ; data labels) in force, area, pressure, peak force, and peak pressure in the lateral compartment as a proportion of the whole joint. Half = one crus transected; Full = entire LCL transected; Prosthetic = prosthetic LCL placed. Force (P = 0.023; –9.0% Δ for full), pressure (P = 0.045; –8.7% Δ for full), peak force (–7.2% Δ) and peak pressure (–7.1% Δ) were significantly reduced in lateral proportion (medial increase) when LCL fully transected (values from Table 5.1). No significant change in contact area. Positive values = increase in lateral proportion from intact; negative = decrease.

Anatomical Location of Peak Contact Pressure

Intra-articular sensor placement within the joint allowed for estimation of sensel location within the joint. Below, in Figure 5.2, is a axial view of a disarticulated canine elbow with pressure mapping data superimposed to demonstrate sensor placement.

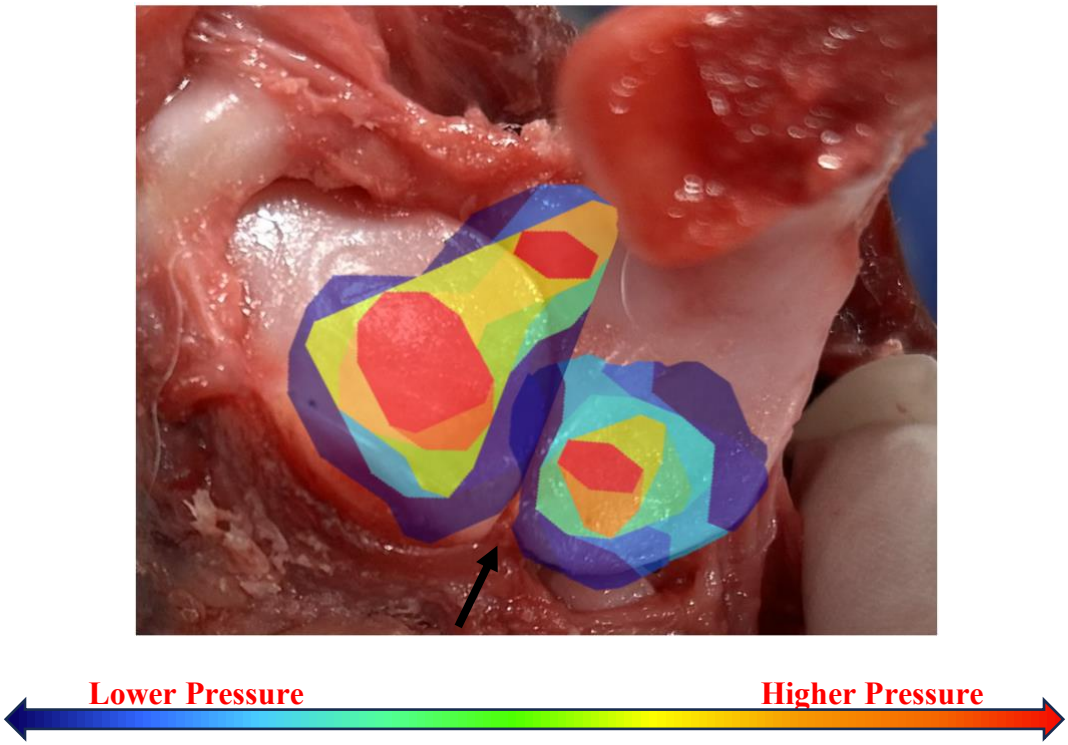

Figure 5.2: Axial view of the disarticulated canine elbow showing the proximal radioulnar joint. The black arrow demonstrates the location of the medial coronoid process. An example of contact map data overlays the joint during loading demonstrating sensor placement within the elbow during experimental testing.

Pressure mapping data showed a caudoaxial increase shift in pressure after transection of the cranial crus of the LCL and complete transection of the LCL in all specimens. Placement of a prosthetic LCL did not restore surface contact areas to that of the intact ligament in any specimen tested. Pressure mapping data can be interpreted in Table 5.2 below by referring to the key contained within the figure.

The centre of force at the time of peak force is denoted by the white boxes in Table 5.2 below. The coordinates for the centre of peak force within the medial compartment did not change between any testing conditions until placement of the prosthetic ligament, however, this was only observed in specimen 3. In this specimen, the centre of force moved caudomedially after placement of the prosthetic LCL. Specimen two was the only specimen observed where the centre of force changed between testing conditions in the lateral compartment. In this specimen, the centre of force shifted progressively more caudoaxial through experimental testing conditions. Variability in peak force centres across specimens precludes firm conclusions on load shifting.

Intact LCL	Cranial Crus of LCL Transected	LCL Transected	Prosthetic Ligament Placed
Specimen 1			
Lateral Medial	Lateral Medial	Lateral Medial	Lateral Medial
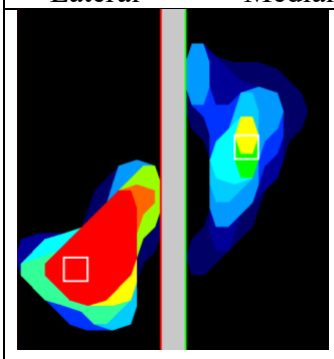	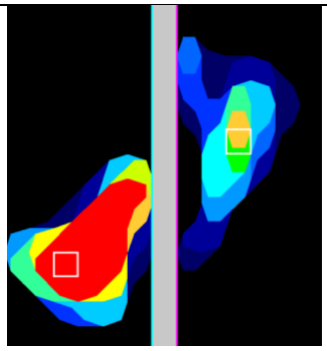	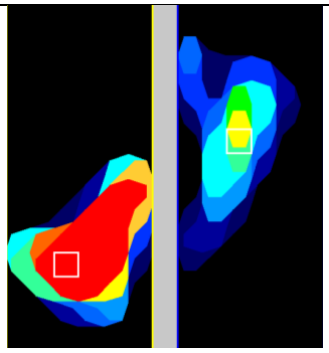	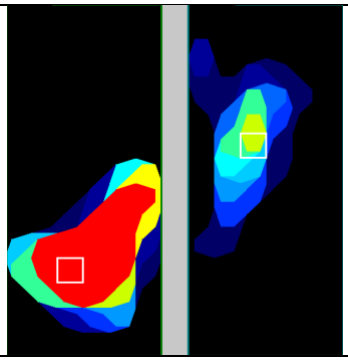
Specimen 2			
Lateral Medial	Lateral Medial	Lateral Medial	Lateral Medial
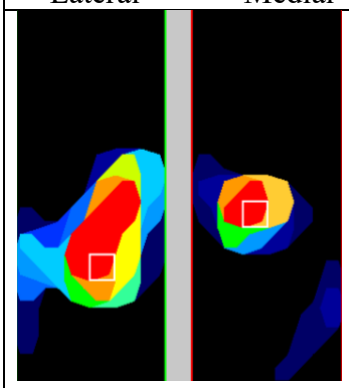	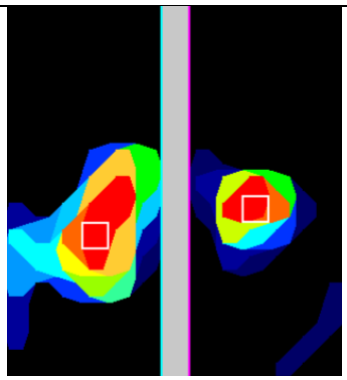	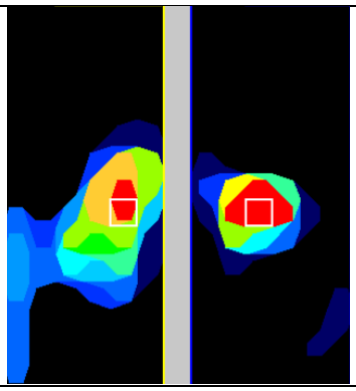	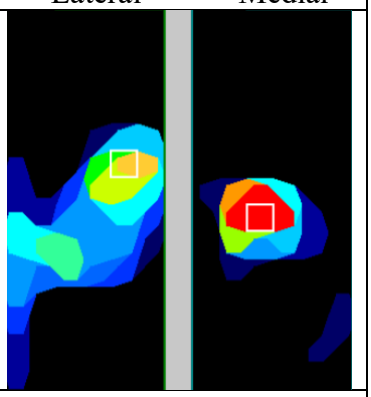
Specimen 3			
Lateral Medial	Lateral Medial	Lateral Medial	Lateral Medial
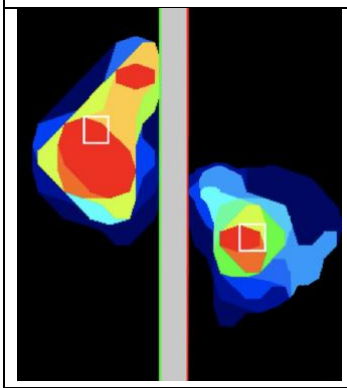	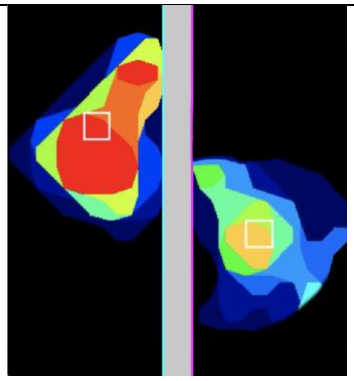	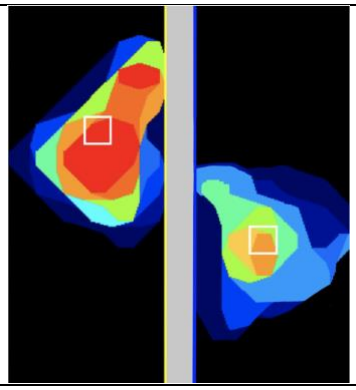	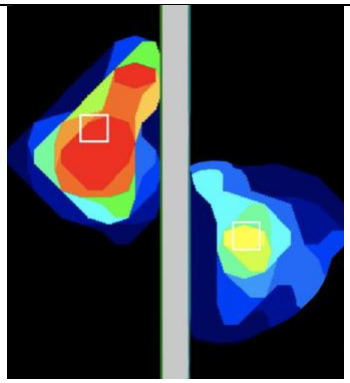

Table 5.2: Intra-articular joint maps showing the area of peak force denoted by the white box in both the medial and lateral compartments when loaded to 200 N for each experimental condition.

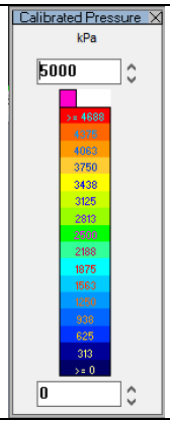

Raw Data

Specimen 1									
Intact									
	Run 1			Run 2			Run 3		
	Whole Joint	Lateral	Medial	Whole Joint	Lateral	Medial	Whole Joint	Lateral	Medial
Force (N)	627.9	477.7	150.2	633.4	483.1	150.4	639.3	487.9	151.4
Contact Area (mm2)	220	114	105	220	114	105	233	114	119
Contact Pressure (kPa)	2860	4184	1425	2885	4231	1427	2747	4273	1277
Peak Force (N)	150.4	150.4	54.1	148.7	148.7	50.9	145.3	145.3	50.3
Peak Contact Pressure (kPa)	8561	8561	3082	8463	8463	2900	8272	8272	2867
Caudal Crus Cut									
Force (N)	644.5	484.2	160.3	638.4	480.8	157.6	644	484.9	159.1
Contact Area (mm2)	233	119	114	237	123	114	228	119	110
Contact Pressure (kPa)	2769	4084	1404	2692	3911	1380	2820	4090	1449
Peak Force (N)	138.8	138.8	52	136.5	136.5	49.7	137.2	137.2	49.3
Peak Contact Pressure (kPa)	7903	7903	2962	7771	7771	2828	7809	7809	2807
LCL Deficient									
Force (N)	652.2	490.3	162	646.7	485.1	161.6	647.9	487.5	160.4
Contact Area (mm2)	233	123	110	237	123	114	237	123	114
Contact Pressure (kPa)	2802	3987	1475	2727	3945	1415	2732	3965	1405
Peak Force (N)	134.8	134.8	49.8	134.2	134.2	48.2	134.2	134.2	47.4
Peak Contact Pressure (kPa)	7676	7676	2833	7638	7638	2746	7638	7638	2698
Prosthetic ligament placed									
Force (N)	658.4	514.6	143.9	652.6	510.9	141.7	650.3	507.8	142.5
Contact Area (mm2)	215	123	92	215	123	92	228	123	105
Contact Pressure (kPa)	3060	4185	1560	3033	4156	1537	2848	4130	1352
Peak Force (N)	133.5	133.5	55.5	134.8	134.8	53.5	136.2	136.2	51.8
Peak Contact Pressure (kPa)	7601	7601	3160	7677	7677	3046	7754	7754	2948
Specimen 2									
Intact									
Force (N)	522.6	324.4	174.3	508.7	315.4	163.7	505.2	326.7	147.8
Contact Area (mm2)	215	101	70	211	101	61	202	101	57
Contact Pressure (kPa)	2429	3212	2481	2413	3123	2662	2501	3235	2589
Peak Force (N)	116.8	116.8	108.8	105.3	105.3	104.5	105.6	105.6	93.6
Peak Contact Pressure (kPa)	6649	6649	6192	5996	5996	5949	6012	6012	5330
Caudal Crus Cut									
Force (N)	505.3	318.1	152.1	484.5	293.8	158.2	473.5	283.6	156.7

Contact Area (mm2)	202	101	61	202	101	61	206	101	61
Contact Pressure (kPa)	2502	3149	2474	2399	2909	2573	2294	2808	2550
Peak Force (N)	99	99	95	94.2	85.7	94.2	95.3	85.2	95.3
Peak Contact Pressure (kPa)	5636	5636	5407	5365	4880	5365	5424	4851	5424
Lateral Collateral Deficient Elbow									
Force (N)	424.8	211.5	163.5	324.6	156.2	164.6	387.6	186.2	158.6
Contact Area (mm2)	206	101	61	149	79	57	202	101	57
Contact Pressure (kPa)	2058	2094	2659	2174	1976	2883	1919	1844	2778
Peak Force (N)	101.1	71.6	101.1	100.7	68.6	100.7	98.7	68.9	98.7
Peak Contact Pressure (kPa)	5757	4078	5757	5732	3906	5732	5619	3922	5619
Prosthetic Ligament Placed									
Force (N)	406.4	203.1	162.5	384.1	185.1	163.2	381.1	179.9	166.8
Contact Area (mm2)	189	97	53	193	105	53	193	105	53
Contact Pressure (kPa)	2152	2102	3084	1988	1757	3098	1972	1708	3165
Peak Force (N)	100.2	72.6	100.2	98.8	62.5	98.8	100.4	59.8	100.4
Peak Contact Pressure (kPa)	5703	4133	5703	5627	3558	5627	5714	3407	5714
Specimen 3									
Intact									
Force (N)	716.4	440.8	179.2	705.5	448.9	187.5	681.9	433.6	191.4
Contact Area (mm2)	281	119	105	285	123	110	285	123	110
Contact Pressure (kPa)	2549	3718	1701	2472	3651	1708	2389	3526	1744
Peak Force (N)	157.7	157.7	77.9	143.4	143.4	76.4	134.8	134.8	74.4
Peak Contact Pressure (kPa)	8979	8979	4435	8162	8162	4348	7672	7672	4233
Caudal Crus Cut									
Force (N)	690.4	437.6	197.3	673.7	431.7	191.2	685.7	437.9	199.3
Contact Area (mm2)	281	119	110	299	127	114	307	132	119
Contact Pressure (kPa)	2457	3691	1798	2256	3390	1675	2231	3324	1681
Peak Force (N)	125.8	125.8	66.6	123.3	123.3	63.2	125.3	125.3	66.9
Peak Contact Pressure (kPa)	7160	7160	3791	7021	7021	3596	7135	7135	3807
LCL Deficient Elbow									
Force (N)	597.2	359.4	187.7	638	389.9	198	616.2	376.7	194.9
Contact Area (mm2)	290	119	119	303	119	123	303	123	123
Contact Pressure (kPa)	2061	3032	1584	2106	3289	1610	2034	3064	1585
Peak Force (N)	100.3	100.3	58.8	108.8	108.8	65.7	107.3	107.3	64.7
Peak Contact Pressure (kPa)	5709	5709	3347	6196	6196	3741	6108	6108	3683
Prosthetic Ligament Placed									
Force (N)	627.5	400.5	182.1	608.4	393.8	175.9	564.9	381	149.6
Contact Area (mm2)	312	127	127	307	123	127	285	123	110

Contact Pressure (kPa)	2013	3145	1430	1979	3203	1382	1979	3099	1363
Peak Force (N)	112.4	112.4	57.7	113.3	113.3	55.5	110.4	110.4	56.5
Peak Contact Pressure (kPa)	6402	6402	3286	6448	6448	3162	6288	6288	3217

Table 5.3: Raw data obtained during experimentation.

Raw Proportion Data

Proportions were calculated as: lateral proportion = lateral compartment value/whole joint value.

Specimen	Condition	Force	Area (mm²)	Pressure (kPa)	Peak Force (N)	Peak Pressure (kPa)
1	Intact	0.761 ± 0.001	0.519 ± 0.015	0.619 ± 0.011	0.928 ± 0.016	0.928 ± 0.016
	Half LCL	0.753 ± 0.002	0.520 ± 0.016	0.620 ± 0.011	0.929 ± 0.007	0.929 ± 0.007
	Full LCL	0.753 ± 0.001	0.527 ± 0.016	0.622 ± 0.011	0.928 ± 0.002	0.928 ± 0.002
	Prosthetic	0.782 ± 0.006	0.576 ± 0.016	0.647 ± 0.016	0.929 ± 0.006	0.929 ± 0.006
2	Intact	0.641 ± 0.010	0.505 ± 0.016	0.680 ± 0.016	0.928 ± 0.054	0.928 ± 0.054
	Half LCL	0.641 ± 0.016	0.505 ± 0.000	0.680 ± 0.016	0.929 ± 0.007	0.929 ± 0.007
	Full LCL	0.545 ± 0.054	0.505 ± 0.072	0.607 ± 0.072	0.929 ± 0.007	0.929 ± 0.007
	Prosthetic	0.514 ± 0.027	0.527 ± 0.016	0.622 ± 0.016	0.929 ± 0.007	0.929 ± 0.007
3	Intact	0.626 ± 0.010	0.428 ± 0.016	0.680 ± 0.016	0.928 ± 0.054	0.928 ± 0.054
	Half LCL	0.641 ± 0.010	0.428 ± 0.016	0.680 ± 0.016	0.929 ± 0.007	0.929 ± 0.007
	Full LCL	0.605 ± 0.027	0.414 ± 0.016	0.680 ± 0.016	0.929 ± 0.007	0.929 ± 0.007
	Prosthetic	0.641 ± 0.016	0.414 ± 0.016	0.680 ± 0.016	0.929 ± 0.007	0.929 ± 0.007

Table 5.4: Raw lateral compartment proportions by specimen and condition (mean of triplicates ± SD)

Chapter 6: Discussion

The aim of this study was to evaluate the contribution of the LCL on intra-articular joint contact mechanics within the medial and lateral compartments in a way that closely resembles the elbow of a live dog. The testing conditions evaluated included the normal joint, the cranial crus of the LCL transected, the LCL transected (both the cranial and caudal crus) and following placement of a prosthetic LCL.

The findings indicated that transection of the entire LCL during axial loading to 200N resulted in a proportional increase in intra-articular force and pressure transmitted through the medial compartment of the elbow. This supports the theory that ligamentous insufficiency alters joint biomechanics and thus load transmission through a joint (34). Interestingly, although force, pressure, peak force and peak pressure all increased proportionally in the medial compartment when the LCL was transected in its entirety, the contact area within the medial compartment did not show any significant change. These findings are consistent with other studies investigating contact mechanics in the normal canine elbow at different angles of flexion, pronation and supination (22). The LCL, as a primary stabiliser of the canine elbow, provides the greatest resistance to supination and provides rotational stability (27). As such, the degree of supination in the lateral collateral deficient elbow can be approximately double that of the intact elbow (28).

Experimentally, Cuddy et. al., demonstrated during supination, similar to our findings, contact area within the medial compartment reduced by 23% (22). In contrast to this study, the present study observed a significant proportional increase in both force and pressure when the LCL was transected in entirety. This observation may be explained by lack of rotational stability provided by the LCL (72). It was hypothesised that a reduction in force in one compartment would correspond to an equal increase in the contralateral compartment which was not observed. This hypothesis was based on findings of another ex vivo study which documented a force shift between compartments after a sliding humeral osteotomy was performed (73). In this model, the anatomical axis was modified as such to shift the magnitude of force within the joint laterally. The increased angle of supination achieved by transection of the LCL, although resulting in a reduction of force transfer through the lateral compartment was not observed to shift to the medial compartment.

Determining the structures which were subject to increased forces is beyond the capabilities of this model. Although the use of tactile sensors is an accepted model to evaluate intra-articular forces, they are limited to the measurement of compressive force only. Considering the functions of the LCL, an ideal experimental model will be capable of measuring compressive, shear and rotational forces transmitted across the joint. Finite element analysis (FEA) represents a potential computational modelling approach to evaluate the biomechanical impact of surgical interventions (such as ligament transection or prosthetic replacement) on joint mechanics, including stress distribution, deformation, and multi-axial loading patterns (74–76). We speculate that forces transmitted through the lateral collateral deficient elbow may be directed through surrounding soft tissue structures or as shearing forces due to the rotational instability observed in these joints. For this reason, these results should be interpreted with caution and further investigations, including FEA models, are warranted to determine the clinical effect transection of the LCL may have on the elbow joint as a whole in vivo.

Another main finding was that placement of a prosthetic LCL did not restore normal joint contact mechanics in this model. Whilst we observed the magnitude of force moved closer to

baseline (the intact elbow) within the medial compartment this finding was not significant. This is not surprising considering degenerative joint disease has been radiographically observed at long term follow-up in 100% of animals after surgical repair and/or augmentation of elbow collateral ligament tears (26). This suggests there is residual instability which is likely to result in clinically significant intra-articular changes and chondrocyte damage despite the reduction of force observed through the lateral compartment in the present study. Our study included only normal canine elbows, we speculate this finding may be augmented in dogs with clinically significant elbow incongruency which has been shown to be associated with joint instability (39,66,77). The role of rotational instability in the transmission of transarticular force is another potential area of future research. In addition, the use of a polypropylene monofilament suture as the prosthetic ligament was likely to have influenced the mechanical behaviour of the construct. Polypropylene has lower stiffness and different creep characteristics than high-stiffness braided ligaments or monofilament nylon leader lines commonly used for collateral ligament replacement, and therefore may not adequately replicate the load–deformation behaviour of the native LCL. This may partly explain the failure of the prosthesis to normalise joint contact mechanics in this model, and should be regarded as a limitation of the study.

Interestingly, the proportional increase in force and pressure was not associated with a significant change in contact area. Investigations in human studies demonstrate that contact area increases with load to distribute stress across a joint an minimise focal areas of high contact pressure (78). In the present study, there was lack of consistent findings between specimens when analysing the co-ordinates for the centre of peak force within each compartment. In two out of the three specimens, partial or complete transection of the LCL did not shift the centre of peak force in the medial compartment which is clinically relevant in cases of MCPD. Mechanical overload has been implicated as one contributor to FMCP, therefore manipulation of both the magnitude and centre of peak force and pressure may be relevant in prevention and treatment for this condition. Pressure maps during maximal axial loading showed a caudoaxial shift in pressure when the LCL was transected in all specimens. This is consistent with findings of another study which showed similar pressure maps in limbs after induced supination (22). Whilst this shows transection may reduce load transmission through the region of the medial coronoid process, these results should be interpreted with caution. Some investigators have suggested that focal regions of increased pressure can be seen in clinical cases of osteoarthritis which may result in unintended pathology after load shifting interventions (22,79). It has been shown in multiple joints in humans, with increasing load, contact area increases to allow for stress distribution across the cartilage interface to minimize focal pressure (80). This is one of the arguments for the theory of dynamic joint incongruence.

This study highlights the complexities of the function of the LCL. There are several limitations to consider when interpreting the results reported here. The use of frozen, thaw cadavers is accepted among researchers and the protocol used in this study for specimen preparation is similar to that of similar studies (22,26,33,34,66–68,70,73,77). Factors beyond reasonable control may have influenced the results of the study by altering the mechanical properties of the specimens. This includes things such as the time between euthanasia and freezing, the duration of freezing and ambient temperature during transport and experimental testing. Variations may have affected tissue degradation and subsequent elastic properties of the soft tissue structures (81,82). As such, findings should be interpreted with caution in light of limitations inherent to all cadaveric freeze, thaw studies.

Dissection of soft tissues proximal to the elbow joint and a medial humeral ostectomy for placement of sensors has been used by other researchers to investigate contact mechanics in the normal dog elbow as well as after interventions aimed at offloading the medial compartment (26,27,33,34,66–68,70,71,73,77,83). Despite this being an accepted model, many in vivo forces involved in weight bearing were not simulated in this model. The triceps myotendinous unit was the only simulated structure in our model. This was based on other studies indicating it is the dominant muscle group supporting the elbow joint in stance (22).

Although by performing an osteotomy to preserve the collateral ligaments, other supporting extra-articular soft tissue structures were disrupted making this model less representative of the live dog elbow. Additionally, although the tactile sensors are incredibly thin and commonly used to measure intra-articular forces, the presence of these alone may have altered measurements. The impact on the sensors was evident after evaluation of sensors after experimental testing in two specimens observed deformation to the plastic outer covering of the sensors themselves. Limitations including human error of sensor placement, variations in elbow flexion angle, variations in experimental technique and anatomic variation between specimens would have been reduced with a larger specimen size. Limbs were loaded to 200 N, although dogs were of similar size, this absolute number was selected based on similar studies (22,26,34). It may have been more clinically relevant to load each limb relative to the body weight of the dog. Peak vertical ground reaction force of the walking and trotting greyhound is 5-7.5 N/kg and 10-12.5 N/kg respectively (34,68). In addition, only one degree of flexion (135 degrees), was evaluated in this study based on the angle of the elbow during the midstance of the gait cycle (84,85). It would be interesting to evaluate if different degrees of elbow flexion affected results in the present study as has been investigated by other groups (22).

The nature of the study design and the practical challenges encountered introduced important limitations to the statistical analysis. No a priori power analysis was performed, and cadaveric limbs underwent rigorous exclusion, resulting in a smaller-than-intended sample size ($n = 3$) for the final data analysis. Post-hoc power estimates of $< 65\%$ and the low degrees of freedom raise concerns about model instability, over-fitting and the possibility of spurious statistically significant findings in the linear model. Although the results should therefore be interpreted with caution, random-effects terms were used to account for between-specimen variation. In retrospect, alternative approaches such as one-sample tests on paired proportions, or non-parametric methods such as the Wilcoxon signed-rank test, may have been more appropriate given the small sample size and the lack of formal normality assessment. The use of parametric methods without testing distributional assumptions introduces additional uncertainty, and the reported P-values should be regarded as exploratory rather than confirmatory. Future studies using similar methodology should aim to include at least 10 specimens, use pre-study power calculations, employ non-parametric or robust statistical methods where appropriate, and ideally incorporate in vivo validation of ex vivo findings.

This study has contributed to the literature in a variety of ways. The method of biomechanical testing was not novel and has been reported in numerous other studies (22,26,33,34,66–68,70–73,77,83). Other reports use a similar model testing experimental conditions which alter the mechanical axis in a way which alters mostly compressive forces across the joint. This study highlights the importance of the LCL as both a primary and secondary stabiliser with further research being warranted to investigate the effects manipulating this structure has on the joint as a whole. Determining a methodology to measure compressive, shear and rotational intra- and extra-articular forces simultaneously as well as how to alter these forces remains an interesting topic for further studies.

Chapter 7: Conclusion

The LCL is a primary stabiliser of the canine elbow joint. In this exploratory ex vivo study LCL transection was associated with proportional increases in medial compartment force and pressure.

Prosthetic replacement showed trends toward partial restoration but not normalisation. The technique of screw placement and prosthetic ligament tensioning was not standardised in this study and warrants further investigation. Furthermore, the mechanical properties of the polypropylene construct used in this study differ from those of both native LCL tissue and clinically used high-stiffness ligament prostheses (e.g. braided ultra-high-molecular-weight polyethylene tapes or nylon leader lines). Future work should incorporate prosthetic materials with stiffness and viscoelastic properties more closely matching those of the native ligament and currently used clinical constructs, and should standardise both prosthesis material and tensioning protocol. During loading of a LCL-deficient elbow in this study, the centre of peak pressure was variable but consistently shifting caudoaxially.

This study introduces the concept that the LCL, as a primary stabiliser of the elbow, influences elbow biomechanics and may also contribute to rotational instability of the humerus in the dog. Clinically this could suggest that laxity of the LCL may be a contributor to the musculotendinous mismatch theory of medial compartment disease in dogs with elbow dysplasia. LCL laxity may contribute to repetitive overloading of the medial compartment in the canine elbow. Over time, resulting in stress microfractures, fragmentation of the coronoid process and subsequent pathology observed in dogs with medial compartment disease. These findings warrant further research with increased numbers of cadaveric specimens, modifications of the current experimental model and refined statistics.

Chapter 8: Abbreviations and Units of Measurement

Abbreviations

MCL	Medial collateral ligament
LCL	Lateral collateral ligament
MCD	Medial coronoid disease
FMCP	Fractured medial coronoid process
CT	Computer tomography
MRI	Magnetic resonance imaging
NSAID	Non-steroidal anti-inflammatory
OA	Osteoarthritis
SHO	Sliding humeral osteotomy
PAUL	Proximal abducting ulnar ostectomy
CUE	Canine unicompartmental elbow arthroplasty
BURP	Biceps ulnar releasing procedure
PUO	Proximal ulnar ostectomy
DUO	Distal ulnar ostectomy
MTS	Materials testing system
SORL	Surgery and Orthopaedics Research Laboratory. Prince of Wales Hospital, NSW, Sydney, Australia.
ID	Identification

Units of Measurement

N	Newtons
A	Acceleration
M	Body of mass
F	Force
V	Voltage
I	Current
R	Resistance
kPa	Kilopascals
Pa	Pascals

Chapter 9: List of Figures and Tables

Figures

Tables

Chapter 10: Conflict of Interest

The author declares no conflict of interest.

Chapter 11: Ethics Approval

Dogs euthanized at an animal shelter facility, for reasons unrelated to the study, were used in accordance with guideline GL001 from the institution's animal ethics committee.

Activities involving only animal tissues or cadavers does not require AEC review where:

(a) The tissues were collected from animals which were already dead; and
(b) Either the animals were not killed for the purposes of teaching or research; or
(c) The animals were killed for a teaching or research purpose already approved by an AEC and in a manner approved by the AEC.

Chapter 12: Author Contributions

Sorcha Rebecca Costello was the lead author, designed the study, collected and organised all data and contributed to statistical analysis. Evelyn Hall also contributed to data analysis. Tian Wang contributed to the experimental design and execution of the experiment. Wendy Baltzer contributed with conceptualisation of the study.

Chapter 13: Acknowledgements

I would like to thank Dr Tian Wang and Dr William Walsh from the University of New South Wales Surgery and Orthopaedics Research Laboratory for their constant support, advice, mentorship and patience during this masters project and for allowing me access to their laboratory to conduct my experiments. I would also like to thank Lance Proctor and James Maxwell for their help in acquiring, selecting and storing specimens for this research. I would like to thank Professor Peter Bennett for his mentorship and advice in construction of this manuscript. I would also like to thank Dr Ruth Zadoks and Dr. Sanaa Zaki for their support and mentorship in navigating this master thesis and guide it to completion. I would also like to acknowledge David Sutton from Bilby Shoes Ltd for supplying sensors from Tekscan Inc and Roksana Sojka Toth for her help in navigating payment for the sensors.

Chapter 14: Funding

Supported by the Sydney University clinical residency program funding.

Chapter 15: References

1. Packard M, Wind A. International Elbow Working Group [Internet]. 2024 [cited 2024 Jun 21]. Available from: http://www.vet-iewg.org
2. Carlson WD, Severin GA. Elbow dysplasia in the dog. A preliminary report. J Am Vet Med Assoc. 1961 Mar 15;138:295–7. PubMed PMID: 13690839.
3. Michelsen J. Canine elbow dysplasia: aetiopathogenesis and current treatment recommendations. Vet J. 2013 Apr;196(1):12–9. doi:10.1016/J.TVJL.2012.11.009 PubMed PMID: 23266351.
4. Bruecker KA, Benjamino K, Vezzoni A, Walls C, Wendelburg KL, Follette CM, et al. Canine Elbow Dysplasia: Medial Compartment Disease and Osteoarthritis. Veterinary Clinics of North America - Small Animal Practice. 2021 Mar 1;51(2):475–515. doi:10.1016/j.cvsm.2020.12.008 PubMed PMID: 33558016.
5. Hebel M, Panek WK, Ruszkowski JJ, Nabzdyk M, Niedzielski D, Pituch KC, et al. Computed tomography findings in a cohort of 169 dogs with elbow dysplasia - a retrospective study. BMC Vet Res. 2021 Dec 1;17(1). doi:10.1186/s12917-021-02997-5 PubMed PMID: 34488762.
6. Danielson KC, Fitzpatrick N, Muir P, Manley PA. Histomorphometry of fragmented medial coronoid process in dogs: A comparison of affected and normal coronoid processes. Veterinary Surgery. 2006 Aug;35(6):501–9. doi:10.1111/j.1532-950X.2006.00183.x PubMed PMID: 16911150.
7. Rohwedder T, Böttcher P. Relation of Computed Tomography-Based Static Axial Radioulnar Incongruence Measurements under General Anaesthesia and Dynamic, in Vivo RUI during the Walk in Canine Elbow Joints with and without Medial Coronoid Process Disease. Veterinary and Comparative Orthopaedics and Traumatology. 2021. doi:10.1055/s-0041-1731811
8. Burton N, Perry M, Fitzpatrick N, Owen M. Comparison of bone mineral density in medial coronoid processes of dogs with and without medial coronoid process fragmentation. Am J Vet Res. 2010;71(1):41–6.
9. Krotscheck U, Kalafut S, Meloni G, Thompson MS, Todhunter RJ, Mohammed HO, et al. Effect of ulnar ostectomy on intra-articular pressure mapping and contact mechanics of the congruent and incongruent canine elbow ex vivo. Veterinary Surgery. 2014;43(3):339–46. doi:10.1111/j.1532-950X.2014.12137.x PubMed PMID: 24467727.
10. Villamonte-Chevalier A, Soler M, Sarria R, Agut A, Latorre R. Anatomical study of fibrous structures of the medial aspect of the canine elbow joint. Veterinary Record. 2012 Dec 1;171(23):596–596. doi:10.1136/VR.100981 PubMed PMID: 23223475.
11. Lewis TW, Ilska JJ, Blott SC, Woolliams JA. Genetic evaluation of elbow scores and the relationship with hip scores in UK Labrador retrievers. The Veterinary Journal. 2011 Aug;189(2):227–33. doi:10.1016/j.tvjl.2011.06.024
12. Woolliams JA, Lewis TW, Blott SC. Canine hip and elbow dysplasia in UK Labrador retrievers. The Veterinary Journal. 2011 Aug;189(2):169–76. doi:10.1016/j.tvjl.2011.06.015
13. Keller G. The use of health databases and selective breeding. St. Louis; 2007.

14. Canine Hip & Elbow Dysplasia Scheme [Internet]. [cited 2026 Apr 10]. Available from: https://www.ava.com.au/about-us/programs-awards/canine-hip-elbow-dysplasia-scheme/
15. Manfredi S, Di Ianni F, Di Girolamo N, Canello S, Gnudi G, Guidetti G, et al. Effect of a commercially available fish-based dog food enriched with nutraceuticals on hip and elbow dysplasia in growing Labrador retrievers. Can J Vet Res. 2018 Apr;82(2):154–8. PubMed PMID: 29755196.
16. Huck J, Biery D, Lawler D, Gregor T, Runge J, Evans R, et al. A Longitudinal Study of the Influence of Lifetime Food Restriction on Development of Osteoarthritis in the Canine Elbow. Veterinary Surgery. 2009 Feb 11;38(2):192–8. doi:10.1111/j.1532-950X.2008.00487.x
17. Meulen G van der. Biomechanical Considerations in Total Elbow Development. In: Advances in Small Animal Total Joint Replacement [Internet]. West Sussex, UK: John Wiley & Sons, Inc.; 2013. p. 163–78. Available from: https://onlinelibrary.wiley.com/doi/10.1002/9781118704776.ch11 doi:10.1002/9781118704776.ch11
18. Duerr FM. Elbow Region. In: Canine Lameness. Wiley; 2020. p. 195–221. doi:10.1002/9781119473992.ch14
19. Baeumlin Y, de Rycke L, van Caelenberg A, van Bree H, Gielen I. Magnetic Resonance Imaging of the Canine Elbow: An Anatomic Study. Veterinary Surgery. 2010 Jul;39(5):566–73. doi:10.1111/j.1532-950X.2010.00690.x PubMed PMID: 20561323.
20. Constantinescu GM, Constantinescu IA. A Clinically oriented comprehensive pictorial review of canine elbow anatomy. Veterinary Surgery. 2009 Feb;38(2):135–43. doi:10.1111/j.1532-950X.2008.00480.x PubMed PMID: 19236670.
21. Lamb CR, Wong K. Ultrasonographic anatomy of the canine elbow. Veterinary Radiology and Ultrasound. 2005 Jul;46(4):319–25. doi:10.1111/j.1740-8261.2005.00060.x PubMed PMID: 16229434.
22. Cuddy LC, Lewis DD, Kim SE, Conrad BP, Banks SA, Horodyski M, et al. Contact mechanics and three-dimensional alignment of normal dog elbows. Veterinary Surgery. 2012 Oct;41(7):818–28. doi:10.1111/J.1532-950X.2012.01036.X PubMed PMID: 22957539.
23. Oliveira D, Baraldi-Artoni S, Shimano A, Rossi J, Tovar M. Role of the oblique ligament in the integrity of the medial collateral ligament of the canine elbow joint [Papel do ligamento oblíquo na integridade do ligamento colateral medial da articulação do cotovelo de cães]. Arq. Bras. Med. Vet. Zootec., v. 2007.
24. Vogelsang RL, Vasseur PB, Peauroi JR, Kass PH, Sharkey N. Structural, material, and anatomic characteristics of the collateral ligaments of the canine cubital joint. Am J Vet Res. 1997 May;58(5). PubMed PMID: 9140551.
25. Duerr FM. Elbow Region. In: Canine Lameness [Internet]. First. John Wiley & Sons, Inc; 2020 [cited 2021 Nov 10]. p. 195–221. Available from: www.wiley.com/go/duerr/lameness
26. Mason DR, Schulz KS, Fujita Y, Kass PH, Stover SM. In vitro force mapping of normal canine humeroradial and humeroulnar joints. Am J Vet Res. 2005 Jan;66(1):132–5. doi:10.2460/AJVR.2005.66.132 PubMed PMID: 15691048.

27. Talcott KW, Schulz KS, Kass PH, Mason DR, Stover SM. In vitro biomechanical study of rotational stabilizers of the canine elbow joint. Am J Vet Res. 2002 Nov 1;63(11):1520–6. doi:10.2460/ajvr.2002.63.1520
28. Campbell JR. Luxation and ligamentous injuries of the elbow of the dog. The Veterinary clinics of North America. 1971. p. 429–40. doi:10.1016/S0091-0279(71)50054-5 PubMed PMID: 4348589.
29. Farrell M, Draffan D, Gemmill T, Mellor D, Carmichael S. In vitro validation of a technique for assessment of canine and feline elbow joint collateral ligament integrity and description of a new method for collateral ligament prosthetic replacement. Veterinary Surgery. 2007 Aug;36(6):548–56. doi:10.1111/j.1532-950X.2007.00281.x PubMed PMID: 17686128.
30. Dickomeit MJ, Böttcher P, Hecht S, Liebich HG, Maierl J. Topographic and age-dependent distribution of subchondral bone density in the elbow joints of clinically normal dogs. Am J Vet Res. 2011 Apr;72(4). doi:10.2460/ajvr.72.4.491
31. Hulse D, Young B, Beale B, Kowaleski M, Vannini R. Relationship of the biceps-brachialis complex to the medial coronoid process of the canine ulna. Vet Comp Orthop Traumatol. 2010;23(3):173–6. doi:10.3415/VCOT-09-06-0063 PubMed PMID: 20422120.
32. Villamonte-Chevalier A, van Bree H, Broeckx BJG, Dingemanse W, Soler M, van Ryssen B, et al. Assessment of medial coronoid disease in 180 canine lame elbow joints: A sensitivity and specificity comparison of radiographic, computed tomographic and arthroscopic findings. BMC Vet Res. 2015 Sep 25;11(1). doi:10.1186/s12917-015-0556-9 PubMed PMID: 26407863.
33. Gutbrod A, Guerrero TG. Effect of external rotational humeral osteotomy on the contact mechanics of the canine elbow joint. Veterinary Surgery. 2012 Oct;41(7):845–52. doi:10.1111/J.1532-950X.2012.00995.X PubMed PMID: 22823108.
34. Preston CA, Schulz KS, Kass PH. In vitro determination of contact areas in the normal elbow joint of dogs. Am J Vet Res. 2000;61(10):1315–21. doi:10.2460/ajvr.2000.61.1315 PubMed PMID: 11039568.
35. MOORES AP, BENIGNI L, LAMB CR. Computed Tomography Versus Arthroscopy for Detection of Canine Elbow Dysplasia Lesions. Veterinary Surgery. 2008 Jun 25;37(4):390–8. doi:10.1111/j.1532-950X.2008.00393.x
36. Meyer-Lindenberg A, Felir M, Molte I. Short- and long-term results after surgical treatment of an ununited anconeal process in the dog. Veterinary and Comparative Orthopaedics and Traumatology. 2001 Feb 9;14(02):101–10. doi:10.1055/s-0038-1632683
37. House MR, Marino DJ, Lesser ML. Effect of limb position on elbow congruity with CT evaluation. Vet Surg. 2009 Feb;38(2):154–60. doi:10.1111/j.1532-950X.2008.00482.x PubMed PMID: 19236672.
38. Mason DR, Schulz KS, Samii VF, Fujita Y, Hornof WJ, Herrgesell EJ, et al. Sensitivity of radiographic evaluation of radio-ulnar incongruence in the dog in vitro. Vet Surg. 2002;31(2):125–32. doi:10.1053/jvet.2002.31046 PubMed PMID: 11884957.
39. Samoy Y, Van Ryssen B, Gielen I, Walschot N, Van Bree H. Review of the literature: Elbow incongruity in the dog. Veterinary and Comparative Orthopaedics and Traumatology. 2006;19(1):1–8. PubMed PMID: 16594537.

40. Fitzpatrick N, Yeadon R. Working algorithm for treatment decision making for developmental disease of the medial compartment of the elbow in dogs. Veterinary Surgery. 2009;38(2):285–300. doi:10.1111/j.1532-950X.2008.00495.x PubMed PMID: 19236686.
41. Rohwedder T, Fischer M, Böttcher P. In vivo fluoroscopic kinematography of dynamic radio-ulnar incongruence in dogs. Open Vet J. 2017 Jul 23;7(3):221–8. doi:10.4314/ovj.v7i3.4
42. Temwichitr J, Leegwater PAJ, Auriemma E, van't Veld EM, Zijlstra C, Voorhout G, et al. Evaluation of radiographic and genetic aspects of hereditary subluxation of the radial head in Bouviers des Flandres. Am J Vet Res. 2010 Aug;71(8). doi:10.2460/ajvr.71.8.884
43. Vezzoni A, Benjamino K. Canine Elbow Dysplasia. Veterinary Clinics of North America: Small Animal Practice. 2021 Mar;51(2):439–74. doi:10.1016/j.cvsm.2020.12.007
44. Cook C, Cook J. Diagnostic Imaging of Canine Elbow Dysplasia: A Review. Veterinary Surgery. 2009 Feb 11;38(2):144–53. doi:10.1111/j.1532-950X.2008.00481.x
45. Burton NJ, Warren-Smith CMR, Roper DP, Parsons KJ. CT assessment of the influence of dynamic loading on physiological incongruency of the canine elbow. Journal of Small Animal Practice. 2013 Jun;54(6):291–8. doi:10.1111/jsap.12093 PubMed PMID: 23710691.
46. Burton NJ, Owen MR, Kirk LS, Toscano MJ, Colborne GR. Conservative Versus Arthroscopic Management for Medial Coronoid Process Disease in Dogs: A Prospective Gait Evaluation. Veterinary Surgery. 2011 Dec 23;40(8):972–80. doi:10.1111/j.1532-950X.2011.00900.x
47. Böttcher P. Accelerated cartilage loss following subtotal coronoid ostectomy. In: Proceedings of the American College of Veterinary Surgeons Symposium. Chicago; 2011. p. 108–9.
48. Fitzpatrick N, Caron A, Solano MA. Bi-Oblique Dynamic Proximal Ulnar Osteotomy in Dogs: Reconstructed Computed Tomographic Assessment of Radioulnar Congruence over 12 weeks. Veterinary Surgery. 2013 Aug 29;42(6):727–38. doi:10.1111/j.1532-950X.2013.12014.x
49. Serrani D, Sassaroli S, Gallorini F, Salvaggio A, Tambella AM, Biagioli I, et al. Clinical and Radiographic Evaluation of Short- and Long-Term Outcomes of Different Treatments Adopted for Elbow Medial Compartment Disease in Dogs. Vet Sci. 2022 Feb 7;9(2):70. doi:10.3390/vetsci9020070
50. Fitzpatrick N, Bertran J, Solano MA. Sliding Humeral Osteotomy: Medium-Term Objective Outcome Measures and Reduction of Complications With a Modified Technique. Veterinary Surgery. 2015 Feb 30;44(2):137–49. doi:10.1111/j.1532-950X.2014.12213.x
51. Wendelburg KM, Beale BS. Medium and Long Term Evaluation of Sliding Humeral Osteotomy in Dogs. Veterinary Surgery. 2014 Oct 31;43(7):804–13. doi:10.1111/j.1532-950X.2014.12252.x
52. Vezzoni A. Elbow Techniques Update: PAUL. In: 27th Annual Scientific Meeting of the European College of Veterinary Surgeons. 2018.
53. Cook JL, Schulz KS, Karnes GJ, Franklin SP, Canapp SO, Lotsikas PJ, et al. Clinical outcomes associated with the initial use of the Canine Unicompartmental

Elbow (CUE) Arthroplasty System(®). Can Vet J. 2015 Sep;56(9):971–7. PubMed PMID: 26345493.
54. Preston CA, Schulz KS, Taylor KT, Kass PH, Hagan CE, Stover SM. In vitro experimental study of the effect of radial shortening and ulnar ostectomy on contact patterns in the elbow joint of dogs. Am J Vet Res. 2001 Oct;62(10). doi:10.2460/ajvr.2001.62.1548
55. Farrell M, Draffan D, Gemmill T, Mellor D, Carmichael S. In vitro validation of a technique for assessment of canine and feline elbow joint collateral ligament integrity and description of a new method for collateral ligament prosthetic replacement. Vet Surg. 2007 Aug;36(6):548–56. doi:10.1111/j.1532-950X.2007.00281.x PubMed PMID: 17686128.
56. Morris AS, Langari R. Pressure Measurement. In: Measurement and Instrumentation. Elsevier; 2021. p. 469–97. doi:10.1016/C2018-0-01451-6
57. Morris AS, Langari R. Mass, force, and torque measurement. In: Measurement and Instrumentation. Elsevier; 2021. p. 551–68. doi:10.1016/C2018-0-01451-6
58. Cuddy LC, Lewis DD, Kim SE, Conrad BP, Banks SA, Horodyski M, et al. Contact Mechanics and Three-Dimensional Alignment of Normal Dog Elbows. Veterinary Surgery. 2012 Oct 7;41(7):818–28. doi:10.1111/j.1532-950X.2012.01036.x
59. Lorenz ND, Channon S, Pettitt R, Smirthwaite P, Innes JF. Ex vivo kinematic studies of a canine unlinked semi-constrained hybrid total elbow arthroplasty system. Veterinary and Comparative Orthopaedics and Traumatology. 2015 Dec 26;28(01):39–47. doi:10.3415/VCOT-14-01-0002
60. Rhode M, Harms O, Finck Y, Dautzenberg P, Schweizer J, Lüpke M, et al. Performing a Three-Dimensional Finite Element Analysis to Simulate and Quantify the Contact Pressure in the Canine Elbow Joint: A Pilot Study. Veterinary and Comparative Orthopaedics and Traumatology. 2022 Sep 4;35(05):279–88. doi:10.1055/s-0042-1748876
61. Gutbrod A, Guerrero TG. Effect of External Rotational Humeral Osteotomy on the Contact Mechanics of the Canine Elbow Joint. Veterinary Surgery. 2012 Oct 23;41(7):845–52. doi:10.1111/j.1532-950X.2012.00995.x
62. Krotscheck U, Kalafut S, Meloni G, Thompson MS, Todhunter RJ, Mohammed HO, et al. Effect of Ulnar Ostectomy on Intra-Articular Pressure Mapping and Contact Mechanics of the Congruent and Incongruent Canine Elbow *Ex Vivo*. Veterinary Surgery. 2014 Apr 27;43(3):339–46. doi:10.1111/j.1532-950X.2014.12137.x
63. Lee MH, Nicholls HR. Review Article Tactile sensing for mechatronics—a state of the art survey. Mechatronics. 1999 Feb;9(1):1–31. doi:10.1016/S0957-4158(98)00045-2
64. Chen H, Zhou Y. Introduction to tactile sensors. In: Functional Tactile Sensors. Elsevier; 2021. p. 1–12. doi:10.1016/C2019-0-01971-1
65. Aspinall V, Cappello M. The Dog and Cat Muscular System. In: Introduction to Animal and Veterinary Anatomy and Physiology. Oxford: CAB International; 2019. p. 100–17.
66. Mcconkey MJ, Valenzano DM, Wei A, Li T, Thompson MS, Mohammed HO, et al. Effect of the Proximal Abducting Ulnar Osteotomy on Intra-Articular Pressure Distribution and Contact Mechanics of Congruent and Incongruent

Canine Elbows Ex Vivo. Vet Surg. 2016 Apr 1;45(3):347–55. doi:10.1111/VSU.12456 PubMed PMID: 27007191.
67. Crystal E, Brettle A, Maddox TW, Jones D, Walton MB. Effect of Medial Opening Wedge and External Rotational Humeral Osteotomies on Medial Elbow Compartment Pressure: An Ex Vivo Study. Veterinary and Comparative Orthopaedics and Traumatology. 2023;37(04):196–205. doi:10.1055/S-0044-1779711/ID/JR23030032-26/BIB PubMed PMID: 38395060.
68. Preston CA, Schulz KS, Taylor KT, Kass PH, Hagan CE, Stover SM. In vitro experimental study of the effect of radial shortening and ulnar ostectomy on contact patterns in the elbow joint of dogs. Am J Vet Res. 2001 Oct 1;62(10):1548–56. doi:10.2460/AJVR.2001.62.1548 PubMed PMID: 11592318.
69. Varner C, Dixon L, Simons MC. The Past, Present, and Future: A Discussion of Cadaver Use in Medical and Veterinary Education. Front Vet Sci. 2021 Nov 10;8. doi:10.3389/fvets.2021.720740
70. Mason DR, Schulz KS, Fujita Y, Kass PH, Stover SM. Measurement of humeroradial and humeroulnar transarticular joint forces in the canine elbow joint after humeral wedge and humeral slide osteotomies. Veterinary Surgery. 2008 Jan;37(1):63–70. doi:10.1111/J.1532-950X.2007.00349.X PubMed PMID: 18199058.
71. Fujita Y, Schulz KS, Mason DR, Kass PH, Stover SM. Effect of humeral osteotomy on joint surface contact in canine elbow joints. Am J Vet Res. 2003 Apr 1;64(4):506–11. doi:10.2460/AJVR.2003.64.506 PubMed PMID: 12693544.
72. Rohwedder T. Biomechanics of the Canine Elbow Joint. In: Rutland C, editor. Updates on Veterinary Anatomy and Physiology. Intechopen; 2021. p. 1–24.
73. Breiteneicher AH, Norby B, Schulz KS, Kerwin SC, Hulse DA, Fox DB, et al. The Effect of Sliding Humeral Osteotomy (SHO) on Frontal Plane Thoracic Limb Alignment: An Ex Vivo Canine Cadaveric Study. Veterinary Surgery. 2016 Nov 1;45(8):1095–107. doi:10.1111/VSU.12574 PubMed PMID: 27735063.
74. Brown NP, Bertocci GE, Marcellin-Little DJ. Canine stifle joint biomechanics associated with tibial plateau leveling osteotomy predicted by use of a computer model. Am J Vet Res. 2014;75(7):626–32. doi:10.2460/AJVR.75.7.626 PubMed PMID: 24959728.
75. Brown NP, Bertocci GE, Marcellin-Little DJ. Influence of biomechanical parameters on cranial cruciate ligament-deficient or -intact canine stifle joints assessed by use of a computer simulation model. Am J Vet Res. 2015 Nov 1;76(11):952–8. doi:10.2460/AJVR.76.11.952 PubMed PMID: 26512540.
76. Brown NP, Bertocci GE, Marcellin-Little DJ. Development of a Canine Stifle Computer Model to Evaluate Cranial Cruciate Ligament Deficiency. https://doi.org/101142/S0219519413500437. 2013 Apr 11;13(2). doi:10.1142/S0219519413500437
77. Krotscheck U, Kalafut S, Meloni G, Thompson MS, Todhunter RJ, Mohammed HO, et al. Effect of ulnar ostectomy on intra-articular pressure mapping and contact mechanics of the congruent and incongruent canine elbow ex vivo. Veterinary Surgery. 2014;43(3):339–46. doi:10.1111/J.1532-950X.2014.12137.X PubMed PMID: 24467727.

78. Halls AA, Travill A. TRANSMISSION OF PRESSURES ACROSS THE ELBOW JOINT. Anat Rec. 1964;150(3):243–7. doi:10.1002/AR.1091500305 PubMed PMID: 14227963.
79. Andriacchi TP, Mündermann A, Smith RL, Alexander EJ, Dyrby CO, Koo S. A framework for the in vivo pathomechanics of osteoarthritis at the knee. Ann Biomed Eng. 2004 Mar;32(3):447–57. doi:10.1023/B:ABME.0000017541.82498.37 PubMed PMID: 15095819.
80. Matsuki KO, Matsuki K, Mu S, Sasho T, Nakagawa K, Ochiai N, et al. In vivo 3D kinematics of normal forearms: analysis of dynamic forearm rotation. Clin Biomech (Bristol, Avon). 2010 Dec;25(10):979–83. doi:10.1016/J.CLINBIOMECH.2010.07.006 PubMed PMID: 20696507.
81. Blaker CL, Ashton DM, Hartnell N, Little CB, Clarke EC. Tendon biomechanical properties are altered by storage duration but not freeze-thaw temperatures or cycles. Journal of Orthopaedic Research®. 2024 Jun 1;42(6):1180–9. doi:10.1002/JOR.25783 PubMed PMID: 38245841.
82. Gottsauner-Wolf F, Grabowski JJ, Chao EYS, An K -N. Effects of freeze/thaw conditioning on the tensile properties and failure mode of bone-muscle-bone units: a biomechanical and histological study in dogs. J Orthop Res. 1995;13(1):90–5. doi:10.1002/JOR.1100130114 PubMed PMID: 7853109.
83. Rhode M, Harms O, Finck Y, Dautzenberg P, Schweizer J, Lüpke M, et al. Performing a Three-Dimensional Finite Element Analysis to Simulate and Quantify the Contact Pressure in the Canine Elbow Joint: A Pilot Study. Vet Comp Orthop Traumatol. 2022 Sep 1;35(5):279–88. doi:10.1055/S-0042-1748876 PubMed PMID: 35785818.
84. Sandberg GS, Torres BT, Budsberg SC. Review of kinematic analysis in dogs. Veterinary Surgery. 2020 Aug 1;49(6):1088–98. doi:10.1111/vsu.13477 PubMed PMID: 32609926.
85. Allen K, DeCamp CE, Braden TD, Balms M. Kinematic Gait Analysis of the Trot in Healthy Mixed Breed Dogs. Veterinary and Comparative Orthopaedics and Traumatology. 1994;07(04):148–53. doi:10.1055/S-0038-1633088